LITHOS 348-349 (2019) 105179

Contents lists available at ScienceDirect

LITHOS

journal homepage: www.elsevier.com/locate/lithos

Trace element discrimination of arc, slab failure, and A-type granitic rocks

Joseph B. Whalen [a, *], Robert S. Hildebrand [b]

[a] Geological Survey of Canada, 601 Booth Street, Ottawa, Ontario K1A 0E8, Canada
[b] 1401 N. Camino de Juan, Tucson, AZ 85745, USA

ARTICLE INFO

Article history:
Received 23 May 2019
Received in revised form
21 August 2019
Accepted 22 August 2019
Available online 28 August 2019

Keywords:
Slab failure
I-types
A-types
Trace elements
Discrimination diagrams
Tectonic settings

ABSTRACT

Although widely used, classification schemes for granitic rocks have until now failed to separate slab failure from arc magmatism in collisional orogens. Our previous work showed that Cretaceous Cordilleran-type batholiths are composed of a pre-collisional belt of mesozonal to epizonal arc plutons, commonly emplaced into their own cover, and a post- accretion tract of what we interpret as "slab failure" plutons, emplaced into the tectonically thickened collisional hinterland. Histograms based on new geochemical compilations of pre- and post-collisional igneous rocks were employed to derive trace element criterion to distinguish between these two plutonic types. Using rocks over the SiO_2 range of 55 −70 wt. % and aluminum saturation index of <1.1, slab failure rocks are readily separated from arc rocks based on Sr/Y > 20, Nb/Y > 0.4, Ta/Yb > 0.3, La/Yb > 10, Gd/Yb > 2, and Sm/Yb > 2.5. Also, we found that A-type magmas can be distinguished from other post-collisional igneous rocks based on Ta + Yb>6 ppm and Nb + Y > 60 ppm. These trace element differences between our pre-collisional arc and post-collisional slab failure plus A-type groups allowed us to build composite discrimination diagrams for destructive margin igneous rocks. Although most S-type granites are also post-collisional, they should not be plotted on our diagrams, for some of their geochemical features overlap those of our slab failure group. Unlike our arc and slab failure groups, A-type granites are formed in diverse tectonic settings such that their classification is more related to geochemical signature and magma sources than to tectonic setting. Lastly, we show how our discrimination diagrams delineate examples of slab failure magmatism through time and suggest links with porphyry Cu-Au deposits.

1. Introduction

Over the last 40 years, geologists attempted to classify granitoid rocks using a variety of schemes. In doing so, they assumed that features, such as textures, modal mineralogy, geochemistry and isotopes would elucidate tectonic setting and, ultimately, their origin. Commonly used major element approaches include the source based I-/S- scheme of Chappell and White (1974, 2001), multicationic parameter schemes (Batchelor and Bowden, 1985; Debon and LeFort, 1983), and a multicomponent approach (Frost et al., 2001; Frost and Frost, 2008, 2011). Granitoid classifications using discrimination diagrams based on trace element abundances and ratios include: (a) A-type granite discrimination plots (Eby, 1990, 1992; Whalen et al., 1987) that can provide information on magma sources and constrain tectonic setting; and (b) a tectono-magmatic scheme (Pearce, 1996; Pearce et al., 1984) that divides granitoid rocks into three orogenic rock types (volcanic arc; syn-collisional; and post-collisional) and two non-orogenic rock types (within-plate and oceanic-ridge). A major flaw of these earlier classification schemes is that they do not recognize slab failure, which plays an important role in the generation of granitoid magmatism at destructive plate margins.

In recent contributions, we presented a model in which Cordilleran-type batholiths are generated by combinations of two fundamentally different kinematic processes: (1) subduction and (2) slab break-off. Each process commonly yields unique and distinct magmas reflecting derivation from different sources and emplacement into contrasting tectonic regimes at different times relative to deformation (Hildebrand and Whalen, 2014a, 2014b, 2017). We studied the geochemistry of magmatism before and after collisional deformation, and found that trace elements can be used to distinguish between arc and slab failure-related granitoids.

Here we extend our earlier results to include granitoid rocks generated in late post-collisional and anorogenic settings, that is the within-plate granite type of Pearce et al. (1984) and/or the A-

* Corresponding author.

https://doi.org/10.1016/j.lithos.2019.105179
0024-4937/

type granite type of Whalen et al. (1987) and Eby (1990, 1992). As the existence and characteristics of slab failure magmatism are underappreciated, it is necessary to first summarize the geological context of arc and slab failure magmatism, along with a review of the geological and geochemical basis for distinguishing the two types of orogenic granitoid magmatism derived from our study of the Peninsular Ranges Batholith (Hildebrand and Whalen, 2014b). Subsequently, we briefly review granitoid petrogenetic options, introduce our new tectonomagmatic discrimination plots, point out examples of slab failure magmatism over time, and discuss a possible link between slab failure magmatism and mineralized porphyry systems.

2. Destructive margin magmatism: geological context

Since the early work of Hamilton (1969), most geologists believe that Cordilleran batholiths - and by analogy all large, elongate batholiths - were generated by rising arc magmas and consequent crustal melting and mixing above subduction zones in high-standing regions of great crustal thickness, such as the Andes (e.g. Bateman, 1992; Ducea, 2001; Ducea et al., 2015). The Andean batholithic model was based largely on that region's subduction-related volcanism, high general elevation, thick crust, linear nature close to continental margin, and apparently continuous magmatism through time.

Hildebrand and Whalen's (2017) evaluation of arcs and crustal growth concluded that the Andean subduction model is largely incorrect. This assessment is supported by the observation that the majority of currently active continental arcs are, contrary to the Andean paradigm, characterized by sequences of rocks erupted and deposited within subsiding basins, not volcanoes sitting on high-standing thick crust (Busby-Spera, 1988; Hildebrand and Bowring, 1984). Recent examples include: (a) both the modern and ancestral Miocene Cascades, where the volcanoes and their debris aprons subsided in grabens (Williams and McBirney, 1979); (b) the low-standing Alaskan Peninsula (Burk, 1965), where volcanoes such as Augustine are located in Cook Inlet (Power et al., 2010); (c) the Kamchatka Peninsula of easternmost Russia, where stratovolcanoes erupt in extensive fault-bounded troughs close to sea level (Levin et al., 2002); (d) the North Island of New Zealand, where the Taupo zone sector of the arc is actively extending as calderas and stratocones erupt (Harrison and White, 2006); (e) the Central American arc, where volcanoes are aligned in a long, linear, low-standing depression (Williams and McBirney, 1979); and (f) the Hellenic arc, where volcanoes form islands in the Aegean Sea (Druitt and Francaviglia, 1992).

Furthermore, the stratigraphy within pendants and wall rocks of Cordilleran batholiths provides no evidence for thickened crust during arc volcanism, as pre-collisional volcanic rocks are commonly intercalated with shallow-marine sedimentary rocks, and therefore sat at, or below, sea level during volcanism. For example, the Sierra Nevadan arc was demonstrably low standing during volcanism, because its volcanic rocks are intercalated with marine rocks as young as 100 Ma (Memeti et al., 2010; Saleeby et al., 2008). Likewise, in the western Peninsular Ranges, arc volcanic rocks are interbedded with sedimentary rocks containing marine fossils (Allison, 1974). In South America, the 9-km-thick Casma arc volcanics, in part the wall rocks for the younger Coastal batholith of Peru, are dominantly marine (Atherton et al., 1985), as are many of the thick Jurassic to Cretaceous arc rocks within the Ocoite arc of northern Chile (Åberg et al., 1984). Even Precambrian continental arcs, such as the Paleoproterozoic Great Bear magmatic zone of the Wopmay Orogen, were characterized as low-standing zones of subsidence during magmatism (Hildebrand and Bowring, 1984). Thus, where arcs are concerned, the high-standing Andes are an outlier, atypical of both modern and ancient arcs, likely because they were built atop a Late Cretaceous–Paleogene collisional belt (Hildebrand and Whalen, 2014a). Overall, the low-standing nature of arcs differs from collision zones, which are typically regions of abnormally thick crust, rapid exhumation, and a compositionally different suite of magmatic rocks.

In his comprehensive treatise on the origin of granite, Pitcher (1993) partly anticipated our ideas when he wrote "*I have found many of the conclusions of modern studies rather unexpected - that is, that the plate edge batholiths were derived largely as a mantle extract, not from old crust, that they were born in an extensional tectonic environment with all the processes of differentiation taking place at depth and near the source, and that such batholiths are not the true roots of volcanic arcs.*"

Due to the buoyancy contrast between oceanic and continental lithosphere every collision that entails the closure of an ocean basin wide enough to drive collision, must involve break-off of the subducting slab, typically near the oceanic-continental join. Slab failure and break-off are an integral component of plate tectonics and a natural consequence of subduction (Davies and von Blanckenburg, 1995; Sacks and Secor Jr., 1990), which is why continents are old and oceans young. The basic temporal progression relates directly to tectonic control by ocean closing and progresses from subduction-related to slab failure magmatism (Fig. 1).

During arc-continent collision, continental margins are pulled beneath arcs, so magmatism related to the failure of the subducting slab is emplaced into rising, tectonically thickened crust in great contrast to the older arc magmatism erupted onto and/or emplaced into normal to extensionally thinned upper plate crust. Once the slab tears and the lower plate is detached from its oceanic anchor, the trench dies, and rocks of the partially subducted continental margin rise due to buoyancy forces, This elevates the collision zone and leads to erosion of the mountainous hinterland, causing flysch sedimentation to switch to molasse (Wilmsen et al., 2009).

While it is commonly assumed that asthenosphere rising through the tear adiabatically melts, and invades the subcontinental lithospheric mantle (SCLM) and the overlying crust, our studies (Hildebrand and Whalen, 2017) suggest that: (1) it is the metabasaltic-gabbroic upper portion of the torn slab that melts; (2) the resulting magmas rise into, and interact with, the SCLM; and (3) little continental crust is involved. As the magmas intrude the collision zone, they tend to form a linear belt alongside the eroded arc and appear temporally continuous with the older magmatism, and so can be readily confused with it. Due to their location and short-lived, generally voluminous character, slab break-off magmatism is commonly misinterpreted as a 'flare-up' in arc activity (e.g. Lee and Lackey, 2015; Wilkinson, 2013).

Thus, in their simplest form, we envision large continental margin batholiths to be composed of two parts: an older belt of mesozonal to epizonal arc plutons commonly emplaced into their own cover, followed closely by a parallel belt of generally more deeply seated plutons emplaced during crustal thickening and exhumation. More complex scenarios, such as found in the Coast Batholith of British Columbia (Stowall et al., 2019), involve younger arc magmatism due to subduction reversal following collision and possible dismemberment and translation along orogen-parallel strike-slip faults (Hildebrand, 2015; Hildebrand and Whalen, 2014a, 2017).

3. Peninsular Ranges Batholith: type composite arc and slab failure Batholith

Our previously published synthesis of the Peninsular Ranges Batholith (Hildebrand and Whalen, 2014b) provides a robust template to resolve the complexities of destructive margin magmatism elsewhere because: (1) the geochemical, isotopic, and geochronological data are modern and of high quality (Gastil et al., 2014; Lee

et al., 2007); and (2) the geology is reasonably well known (Morton and Miller, 2014).

Rocks within the Peninsular Ranges Batholith were deformed at about 100 Ma when volcanic and plutonic rocks of the Alisitos-Santiago Peak arc were thrust eastward over a west-facing carbonate platform. As arc volcanism ceased with the onset of deformation, we interpreted the deformational event as an arc-continent collision formed when a narrow ocean, known as the Bisbee-Arperos seaway, closed by westward subduction beneath the arc.

Geochemical variations in rocks of the Peninsular Ranges Batholith show that pre-collisional plutons (Santa Ana suite), in the age range 130–100 Ma, contain 48 to 77 wt. % SiO_2, whereas the post-collisional 100–83 Ma La Posta suite plutons contain mostly 60–70 wt. % SiO_2, with few rocks of higher silica content. In general, both pre- and post-collisional suites exhibit mainly metaluminous compositions and are amphibole-bearing. Pre-deformational rocks of the Santa Ana suite define the type calcic suite (Frost and Frost, 2008; Whalen and Frost, 2013), whereas the post-deformational La Posta samples exhibit a calcic to calc-alkalic affinity.

In general, when developing our discrimination plots, plutonic suites were initially identified as arc, slab failure- or A-type on the basis of geological information (see Hildebrand and Whalen, 2017), then confirmed as to their granite grouping based on geochemical criterion. Although the best indicator of slab-failure magmatism is its syn- to post- collisional timing, we were able to discriminate between pre-collisional arc rocks and a subgroup of post-collisional rocks, we interpret as slab-failure magmas, by exploiting differences in trace element concentrations. Slab failure rocks are enriched in Sr, Nb, Ta plus Eu and depleted in heavy rare earth elements (HREE) and Y relative to arc rocks. We generated fields empirically on trace-element plots by observing the separation of trace element ratios (La/Yb, Sm/Yb, Gd/Yb, Nb/Y, Ta/Yb and Sr/Y) on histograms for the Peninsular Ranges Batholith to arrive at values that separated the largest numbers of pre- and post-deformational samples (Hildebrand and Whalen, 2014b). Based on these ratios, arc vs. slab-failure discrimination diagrams were developed employing Sr/Y vs. Nb/Y, La/Yb and Gd/Yb, as well as derivative plots of Gd/Yb vs. Nb/Y and La/Y (Fig. 2a, b) that avoided the use of Sr, which is commonly mobile during alteration of high-Sr slab failure suites, especially at $SiO_2 > 70$ wt. %.

In addition to our empirically derived plots we also observed that plots involving Sm/Yb (Fig. 2c), which highlight the differences in depth of melting (Putirka, 1999), do a good job of separating the two suites of plutons within the Peninsular Ranges Batholith. Furthermore, the field boundaries on the Pearce et al. (1984) Nb vs. Y (Fig. 2d) and Ta vs. Yb plots were revised to reflect extensive new data to create more robust arc and slab failure fields. For easy reference all these previously published plots are included in Supplementary file A.

4. Petrogenesis of arc, slab failure and A-type granitoids

Arc magmas are fundamentally different from slab failure magmas in their petrogenesis. Slab failure rocks derive through deep mantle processes that likely include partial melting of the metabasaltic/gabbroic upper portion of the torn slab, leaving a garnet-bearing, plagioclase- free eclogitic residue (Hildebrand and Whalen, 2017). The strong partitioning of heavy rare earth elements (HREE) into residual garnet and absence of Sr- plus Eu-hosting plagioclase, yields distinctive high La/Yb, Sm/Yb, Gd/Yb and Sr/Y ratios and lack of negative Eu anomalies (Eu/Eu*>1.0) on chondrite normalized REE plots of slab failure magmas. Instability of a Ti-rich phase such as rutile, plus residual garnet, yields their high Nb/Y and Ta/Yb ratios. Hildebrand and Whalen (2017) showed that Sr and Nd isotopes in slab failure rocks of the Sierra Nevada and Peninsular Ranges batholiths were similar to Cenozoic basalts of the Snake River Plain, the Big Pine volcanic field and Mesozoic pyroxenites, all of which are interpreted as having Nd and Sr isotopes signatures derived from the subjacent cratonic subcontinental lithospheric mantle (SCLM). This, coupled with mantle-like oxygen isotopic values for many post-collisional Sierran granitoid rocks (Lackey et al., 2008), the extreme variance in Nd and Sr, as well as nearly complete decoupling of most trace elements from major element trends, led Hildebrand et al. (2018) to suggest that rising melts derived from the metabasaltic-gabbroic upper portion of the torn slab interacted with SCLM. In contrast, arc magmas are generated by volatiles streaming from a subducting slab, resulting in partial melting of spinel-plagioclase source rocks with residual pyroxene, plagioclase and rutile (Till et al., 2012; Ulmer, 2001).

Ever since their recognition as a distinct granite type (Loiselle and Wones, 1979), the petrogenesis of A-type granites has been controversial because they share mineralogical and compositional traits, as well as associated basaltic magmatism, yet are emplaced in a variety of environments from continental margin to oceanic island (Collins et al., 1982; Whalen et al., 1987, 1996, 2006; Creaser et al., 1991; Eby, 1990, 1992; Frost and Frost, 2011; and Bonin, 2007). A-types are defined by, and can be distinguished from, I-types based on geochemical criterion, including higher chlorine/fluorine,

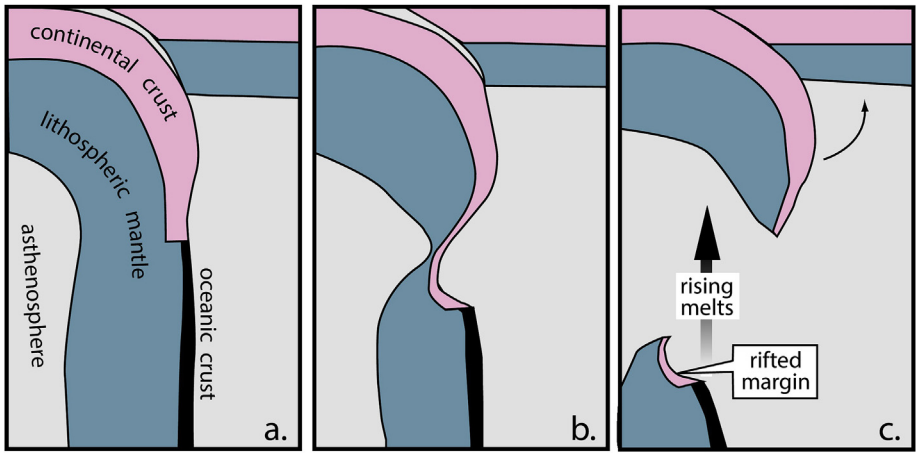

Fig. 1. Sketch illustrating some features of moderately deep slab failure: (a) the leading edge of the continent is subducted beneath the arc; (b) the tearing of the subducting slab largely by ductile necking; and (c) the possibility of the rifted margin tearing from the main continental mass and sinking into the mantle along with the oceanic lithosphere, as suggested by Hildebrand and Bowring (1999). In our model magmas are derived from melting of the upper layers of oceanic crust. Figure adapted from Freeburn et al. (2017).

boron and alkali abundances, lower calcium, aluminum and magnesium contents, higher FeT/Mg ratios and, most distinctively, much higher concentrations of high-field-strength elements, such as zirconium, yttrium, niobium, tantalum and HREE (Dall'Agnol et al., 2012; Pearce et al., 1984; Whalen et al., 1987). Based on contrasting Y/Nb and Yb/Ta signatures, Eby (1990, 1992) subdivided A-type granites into two groups: A1, which has certain geochemical similarities to oceanic-basalts and are inferred to represent intraplate oceanic island and continental rift environments; and A2, which are compositionally closer to average crust and were emplaced during the late stages of collision, perhaps during late-stage extensional collapse. In adopting this scheme, the Y/Nb, value of 1.2 suggested by Eby (1992), inverted to Nb/Y = 0.83, was used to subdivide A1 from A2 subtypes. However, the interpolated equivalent Ta/Yb value of 0.94 did not reliably separate the two A subtypes, possibly because our A-type dataset (see Supplementary file 2) includes samples contaminated by Ta during tungsten carbide mill pulverization. Other trace element ratios (La/Yb, Sm/Yb, Gd/Yb) found to reliably separate arc from slab failure rocks did not separate A1 from A2 groups.

The distinctive geochemistry of A-type granites has resulted in numerous different petrogenetic models (see review of Dall'Agnol et al., 2012). Loiselle and Wones (1979) originally argued that A-type granites developed by fractionation of mantle-derived basalt; similarly, Bonin (2007) suggested that they likely came from mantle-derived, transitional to alkaline, mafic to intermediate, magmas; whereas others (Collins et al., 1982; Windley, 1993) suggested melting of older crustal rocks, such as mafic granulite, was the most appropriate source. Over two decades ago, Whalen et al. (1996) published the results of a detailed geochemical and isotopic (Nd, Sr, O, Pb) study of the ca. 427 Ma Topsails A-type granite suite, Newfoundland Appalachians, and concluded, based on juvenile isotopic signatures, that the origin of this bimodal, but dominantly silicic, magmatic suite lay primarily in the mantle. This conclusion was supported by the basalts, which include tholeiitic, MORB-like, and arc-like compositions, suggesting high degrees of partial melting within both asthenospheric and lithospheric mantle following ca. 460 Ma slab break-off plutonism (Whalen et al., 1997). While the detailed petrogenesis of A-type granitoids remains controversial, they represent a geochemically distinct type of magmatism that occurs both in late post-collisional and anorogenic settings.

5. The problem of S-type granites

Although the protolith-based I- and S-type granite classification scheme of Chappell and White (1974, 2001) is still widely applied by geologists around the world, it is notable that forty years on *"....the most enigmatic granites in relation to origin are the most abundant ones, those belonging to the I-type according to the Chappell-White classification"* (Castro, 2014). This needs to be kept in mind as both arc and slab failure suites are I-type granitic suites, that is, they are derived mainly from sources that were not weathered at the surface. I-type suites have $Na_2O/K_2O>1.0$, aluminum saturation index (ASI) <1.1, and are commonly amphibole-bearing. The differences in trace element ratios that we employed to discriminate arc from slab failure rocks reflect residual pyroxene, plagioclase + rutile and residual garnet without plagioclase and rutile, respectively. In contrast, post-collisional S-type granites are derived mainly from sedimentary protoliths, or other

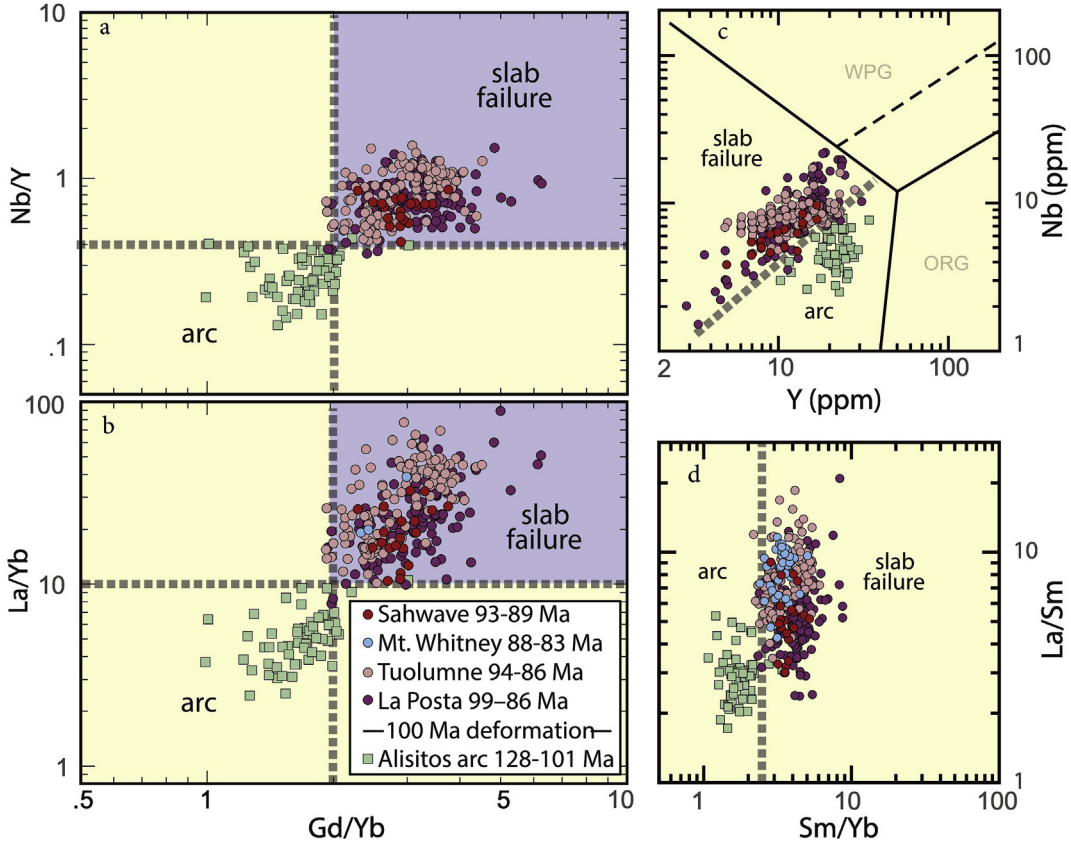

Fig. 2. Plutonic samples with 55 to 70 wt. % SiO_2 from the Peninsular Ranges Batholith (Lee et al., 2007), the Sierra Nevada Batholith (Hirt, 2007; Memeti, 2009) and the Sahwave suite of Nevada (van Buer and Miller, 2010) plotted on tectonomagmatic discrimination plots (Hildebrand and Whalen, 2014b, 2017): (a, b) Gd/Yb vs. Nb/Y and La/Yb; (c) Sm/Yb vs. La/Sm and (d) Y vs. Nb. Note the high degree of separation of arc from slab failure rocks.

rocks that underwent surficial weathering. If partial melting is due to radioactive heating of deeply buried sediments, it can take tens of Myr to reach the point of partial melting (England and Thompson, 1984). S-type granites typically occur in post-collisional settings where they were emplaced during the late stages of orogeny and have a different peralumunous mineralogy and petrogenesis from slab failure magmas, as demonstrated in the Himalayan (Guo and Wilson, 2012) and Variscan (Simons et al., 2016) orogens. Partial melting of weathered feldspar-rich protoliths cannot generate melts that leave a mafic eclogitic restite, as inferred for slab failure magmas (Hildebrand et al., 2018), but instead yield more felsic granulitic feldspar-rich +/- garnet restite. A feldspar-rich restite should preclude high-Sr in the melt to yield rocks with low Sr/Y, whereas residual garnet would likely yield rocks depleted in HREE (elevated La/Yb, Gd/Yb and Sm/ Yb ratios) ratios characteristic of slab failure magmas (Whalen et al., 2018). To better evaluate their potential impact on the recognition of granitoid tectonic settings, data from peraluminous leucogranite suites (see Supplementary file B) were compared to slab failure rocks. On our discrimination plots (Fig. 3) many of these S-type granites exhibit elevated 'slab failure-like' values for La/Yb, Gd/Yb, Sm/Yb and Nb/Y, but have low Sr/Y values, as might be inferred from a granulitic source containing plagioclase and garnet. For this reason, S-types were excluded from our new classification scheme by not plotting samples with SiO_2>70 wt.% and aluminum saturation index (ASI)>1.1 on our diagrams.

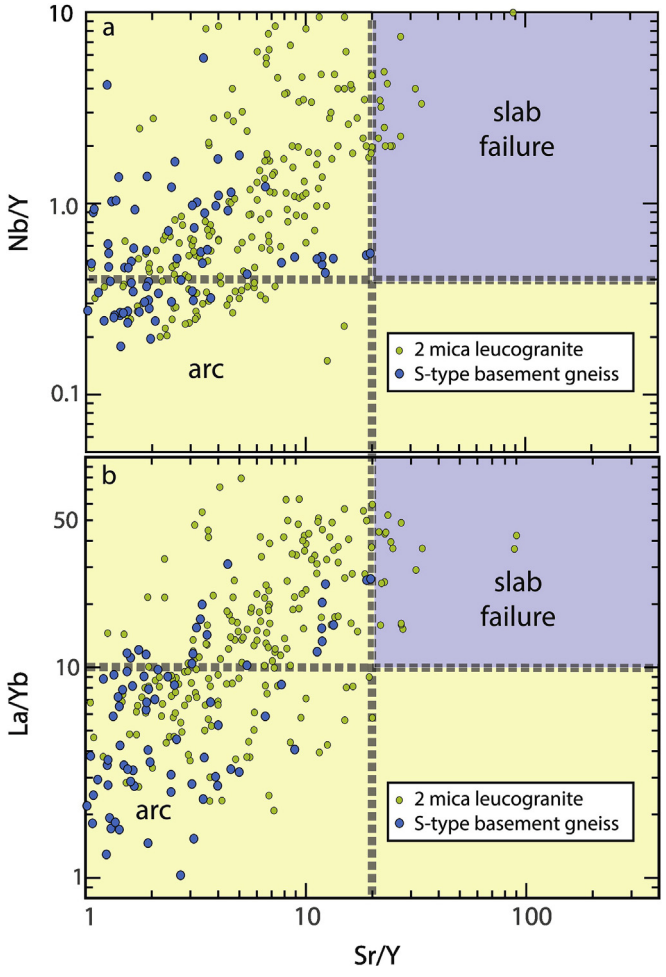

Fig. 3. S-type post-collisional two mica leucogranite and basement gneiss samples plotted on Sr/Y vs. Nb/Y, La/Yb and Gd/Yb slab failure vs. arc trace element ratio discrimination plots of Hildebrand and Whalen (2014b). This plot illustrates how residual garnet and plagioclase without rutile (?) in granulitic restite can impart high Nb/Y, La/Yb and Gd/ Yb, but low Sr/Y, signatures to S-type granite magmas. These plots demonstrate why high aluminum saturation index (ASI) and elevated silica compositions, as shown in Fig. 3, should not be plotted on our new discrimination plots. Otherwise, erroneous interpretations can result.

6. Arc versus slab failure discrimination diagrams: further development and application

To better substantiate our geochemical scheme for distinguishing arc from slab failure magmatism, we compiled modern geochemical datasets of high quality ICP-MS trace element data from active arcs and slab failure settings to compare with rocks of the Peninsular Ranges Batholith (Hildebrand et al., 2018; Hildebrand and Whalen, 2017). The consistency of results (see below) encouraged further investigations.

The combined geological–geochemical approach was first applied to Cretaceous plutonic rocks of the North American Cordillera, which indicated that they are dominantly slab failure, not arc, rocks (Hildebrand and Whalen, 2017). The distribution of units is likely due to the exhumation and erosion of the upper plate arc rocks as the cratonic lower plate rebounded following slab failure. This Cordilleran based study provided a large compilation of slab failure-type granitoid rocks (635 samples) but fewer examples (122 samples) of arc rocks.

Additional geochemical data (see Supplementary file B) from intraoceanic arcs (161 samples) and continental arcs (372 samples) were compiled for this study so as evaluate trace element differences between plutons emplaced in these contrasting tectonic settings. The Aleutians intraoceanic arc is handled separately because its large number of samples (212), would overwhelm smaller datasets derived from other intraoceanic arcs, such as New Britain (Whalen, 1985), Marianas (Johnson, 2014) and supra-subduction zone ophiolites in Oman (Rollinson, 2009) and Elder Creek (Shervais, 2008).

As we wanted to discriminate late-collisional and anorogenic A-type granites from arc and slab failure magmatism, we compiled 443 A-type granite analyses. As Pearce et al. (1984) showed that Y + Nb and Yb + Ta are effective in separating orogenic from within-plate/A-type granitoids, we used histograms of our new data compilations to derive values for these parameters that separate granitoids belonging to our three basic tectonomagmatic groupings (arc, slab failure and A-type) (see Y + Nb histograms in Fig. 4).

The values that separate arc, slab failure and A-type compositions are: Sr/Y (20), Nb/Y (0.4), Ta/Yb (0.3), La/Yb (10.0), Gd/Yb (2.0), Sm/Yb (2.5), Y+Nb (60) and Yb+Ta (6). Most of these values are the same or very similar to those of Hildebrand and Whalen (2014b) which were derived solely from the Peninsular Ranges Batholith (see Supplementary files A and C).

7. Geochemical diversity in slab failure suites

The Cretaceous plutonic rocks of the North American Cordillera contain several distinct suites of post-collisional rocks – the Bayonne, Cassiar, and Selwyn of the Canadian Cordillera and the Ruby batholith of eastern Alaska – that are dominantly epizonal, commonly mineralized, have a broad range of silica with about half the plutons containing SiO_2 > 70 wt. %, and are highly variable with respect to Nd and Sr isotopes (Hildebrand and Whalen, 2017). The more silicic samples examined show reasonable evidence, such as decreasing La/Yb with increasing SiO_2, for rock-fluid interaction (see Fig. 47 of Hildebrand and Whalen, 2017).

To evaluate whether or not major element geochemistry varied systematically between arc and slab failure suites, aluminum saturation index (ASI) was plotted against SiO_2 for these and other data sets (Fig. 5). This exercise highlighted two subgroups within the post-collisional, slab failure rocks: metaluminous to slightly

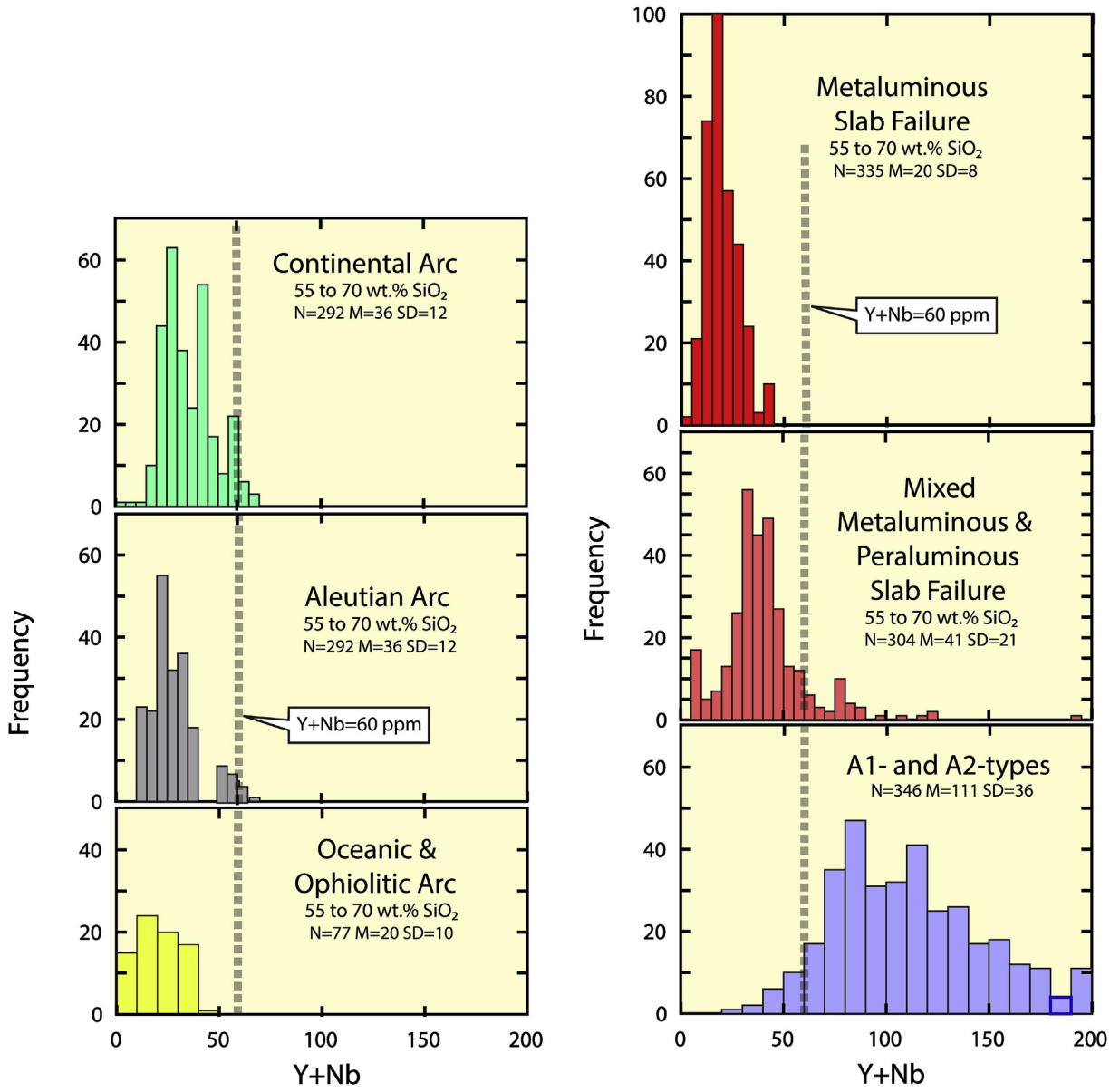

Fig. 4. Y + Nb histograms for arc, slab failure and A-type samples with 55–70 wt. % SiO_2 contents that derive the value of 60 that separates arc and slab failure rocks from A-types employed in the new discrimination diagrams. Included with each histogram are number of samples (N), mean and standard deviation (SD). Similar histograms were used to derive the Ta + Yb value of 6 that separates arc + slab failure compositions from A-types (see Table 2 and Supplementary file C).

peraluminous suites, such as the La Posta, Sierran Crest and Sahwave suites, with aluminum saturation index (ASI) <1.1 and metaluminous to moderately peraluminous suites, such as the Bayonne, Cassiar, Selwyn, and Ruby with ASI mainly <1.0–1.4. Three-quarters of the metaluminous slab failure suite samples contain 55 to 70 wt. % SiO_2, whereas about half of the metaluminous to peraluminous slab failure samples contain >70 wt. % SiO_2. Nearly all of the samples designated as arc rocks contain 55-70 SiO_2, and are metaluminous, whereas >90% of the samples from our S-type, two-mica granite group contain >70 SiO_2 and mostly have ASI >1.1 (Table 2). However, a characteristic of rocks with >70 wt. % SiO_2 temporally and spatially associated with our recognized slab failure rocks is that some of our trace element discrimination ratios are highly variable resulting in many samples plotting outside the slab failure fields (Fig. 6). As these variations are not typical of any recognized type of fractionation, we argued that they were altered by deuteric fluids/and or late-stage ground water circulation (Hildebrand and Whalen, 2017). In contrast, arc samples with SiO_2 >70 wt. % do not show scatter but rather all plot within the arc field (see histogram plots in Supplementary file C).

In the tectonomagmatic discrimination plots of Pearce et al. (1984), their non-orogenic granite group includes both within-plate (herein termed A-type) and ocean-ridge granite subtypes. However, as most ophiolites are now recognized to have formed above subduction zones (MacLeod et al., 2013; Pearce, 2014; Rollinson, 2009; Shervais, 2001, 2008), not at mid-oceanic ridges, we were unable to locate modern high quality ICP-MS granitic data from mid-ocean-ridges, so these ophiolitic granitoid data, which are all characterized by arc signatures, were included in our oceanic/primitive arc compilation. On this basis, we deduced that if granitic rocks do form at mid-oceanic ridges, they are volumetrically very minor and, unless sampled through dredging, would invariably be destroyed by subduction.

Based on our findings regarding high silica S-type granites, and the possibility that many plutonic samples containing less than 55 wt. % SiO_2 are cumulate rocks that do not represent liquid

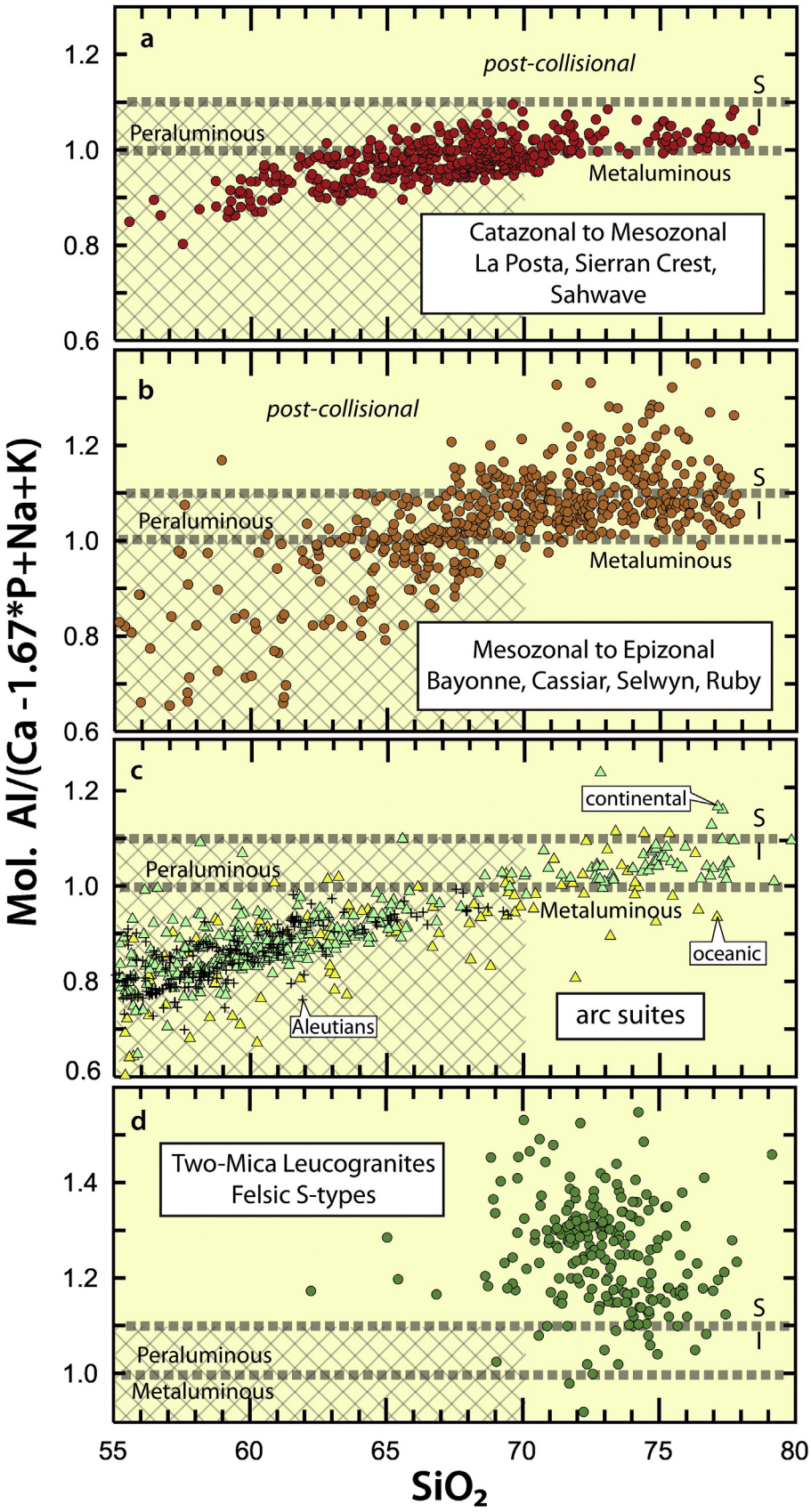

Fig. 5. Aluminum saturation index (ASI) vs. silica plot for: (a) metaluminous to slightly peraluminous post-collisional catazonal to mesozonal granitoids of the La Posta, Sierran Crest and Sahwave plutonic suites; (b) metaluminous to moderately peraluminous post-collisional metazonal to epizonal granitoids of the Bayonne, Cassiar, Selwyn and Ruby suites; (c) arc rocks; and; (d) S-types: two-mica leucogranites and basement S-type granitoid gneisses. The horizontal lines at ASI = 1.1 separates I- from S-type granite compositions (Chappell and White, 1974, 2001) and the hachured boxes show which arc and slab failure granitoid compositions should be plotted on the new trace element ratio discrimination plots, i.e. samples with 55–70 wt. % SiO_2 and ASI < 1.1.

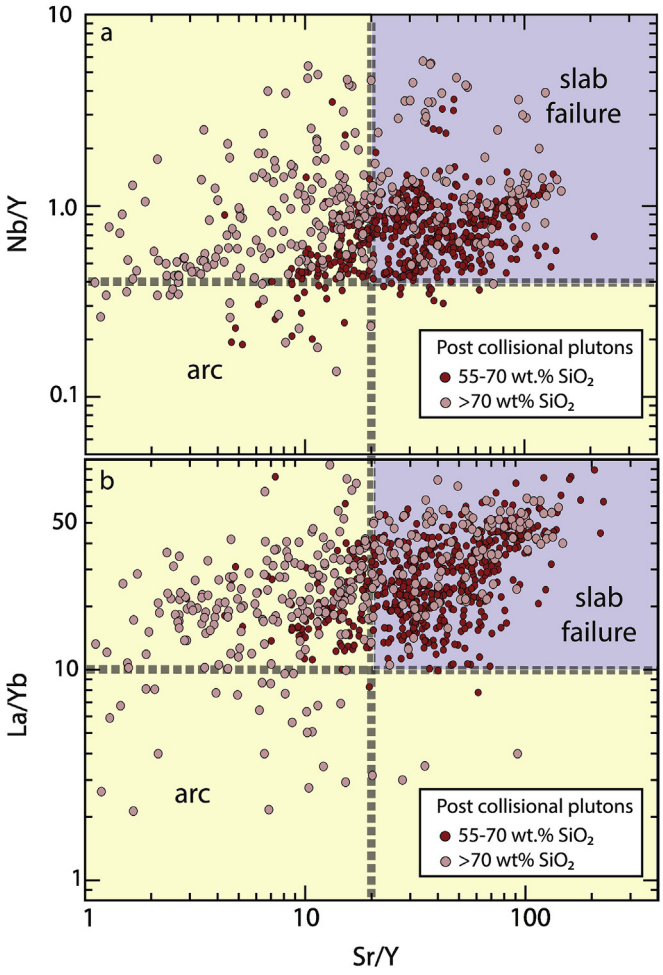

Fig. 6. Sr/Y vs. Nb/Y and La/Yb slab failure vs. arc discrimination plots of Hildebrand and Whalen (2014b) for post-collisional granitoid rocks illustrating the leftward horizontal dispersion to lower Sr/Y values by >70 wt. % SiO_2 slab failure compositions. This behavior is attributed to late fluid-related Sr mobility and argues that Sr/Y is not a robust discriminator between slab failure vs. arc compositions.

compositions, we conclude that our trace element ratio discrimination plots should be restricted to I-type rocks with SiO_2 contents between 55 and 70 wt. % and ASI less than 1.1 (Fig. 3), unless they have Y + Nb > 60 ppm and Ta + Yb > 6 ppm, as those rocks are A-types.

8. Important features of our discrimination plots

1. Samples from both primitive oceanic- and continental-arc rocks plot together in the arc fields on the plots, thus indicating that these plots are not a tool for distinguishing oceanic from continental arc rocks. In fact, the two types of arc rocks are so similar that Hildebrand and Whalen (2017) suggested that assimilation of continental crust may not be a dominant process in arcs built on continental crust.
2. The 55-70 wt. % SiO_2 and ASI filtered metaluminous and metaluminous to peraluminous slab failure compilations closely overlap on these plots indicating that factors causing scatter outside our defined fields are only a problem at high silica values, thus justifying the silica plus ASI filtering approach (see Figs. 3, 4, 5 and 6).
3. The generated field boundaries are horizontal and vertical lines. Thus, granitoid data of unknown tectonic affinity can be readily filtered using spreadsheets into arc, slab failure and A-type compositions.
4. The recommended procedure for handling a granitoid dataset of unknown tectonic setting is as follows: (a) calculate Y + Nb and Yb + Ta in a spreadsheet and sort the granitoid dataset on these parameters. Samples with Y + Nb > 60 and Yb + Ta > 6 ppm are A-types so this subset of samples should not be filtered to remove high-silica or high ASI samples as most A-types contain >70 wt. % silica; (b) filter remainder of samples for 55-70 wt. % SiO_2 and ASI<1.1 to eliminate S-types, cumulate mafic arc, and felsic slab failure samples; (c) plot unfiltered A-types and the rest of the silica and ASI filtered granitoid data on discrimination plots (Figs. 7 and 8) to determine whether they are arc or slab failure compositions. Of note is that, with the exception of Nb/Y and Ta/Yb (cf. Eby, 1990, 1992), trace element ratios employed in Figs. 7 and 8 can't differentiate between late post-collisional A-type suites emplaced following slab failure magmatism (A2 type) or suites that occur in anorogenic/within plate settings such as continental rifts and oceanic islands (A1 type). The A1 and A2 tectonic subdivision of A-types proposed by Eby (1990, 1992) is based on trace element discrimination plots such as triangular Y-Nb-Ce and Y-Nb-3*Ga diagrams.
5. Strontium is commonly mobile in high silica slab failure suites making Sr/Y an unreliable discriminator. We interpret this to reflect fluid alteration of Sr-enriched plagioclase in slab failure rocks, an effect that is not as noticeable in arc rocks because they contain less Sr, presumably due to residual plagioclase in the source. This feature is easily seen on a Sr/Y vs. La/ Yb plot where high silica slab failure samples form a crudely horizontal linear array that transects the arc-slab failure boundary of Sr/Y = 20 on a Sr/Y vs. La/Yb plot, whereas 55–70 wt. % SiO_2 slab failure samples plot almost exclusively in the slab failure field (Fig. 6).
6. Because Sr/Y and La/Yb values in many of the >70 wt. % SiO_2 slab failure plutonic rocks are not correlated, we refrain from calling them 'adakites' or describing them as exhibiting 'adakitic signatures'. According to Moyen (2009), these terms have become so generalized, or confused, that they are being used to describe a far too large group of igneous rocks with their only shared traits being high Sr/Y and La/Yb. Rocks with 'adakitic' compositions can form by various petrogenetic processes, including: (a) partial melting of a high Sr/Y and La/Yb sources; (b) deep high P/T melting of mafic protoliths with abundant residual garnet without plagioclase; (c) fractional crystallization or AFC; and (d) interaction of felsic melts with the mantle (Moyen, 2009.). Based on our analysis, we conclude that slab failure granitoids exhibit most, if not all features attributed to 'adakites', but it does not necessarily follow that all 'adakitic rocks' are products of slab failure.

9. Testing of new discrimination plots

Examination of the new trace element discrimination plots (Figs. 7, 8, Table 2 and Supplementary file D) demonstrates excellent discrimination between arc and slab failure rocks. For the post-collisional samples, 99.6% plot in the slab failure field defined by La/Yb (556 samples), whereas for Ta/Yb 98.2% are classified as slab failure rocks (494 samples). Similarly for the combined arc sample set, of 813 samples with La/Yb, 99.8% plot in the arc field, whereas of the 734 samples with Ta/Yb, 99.2% plot as arc samples. These plots also do a good job of separating slab failure plus arc samples from A-type samples in that of 1200 arc plus slab failure samples, only 2.5% are misclassified as A-type granites. Plots in Supplementary file 4 and statistics in Table 2 also provide visual and statistical justification for our restricting plotted arc and slab failure samples to <70 wt. % SiO_2 compositions (see Fig. 4). Using La/Yb as

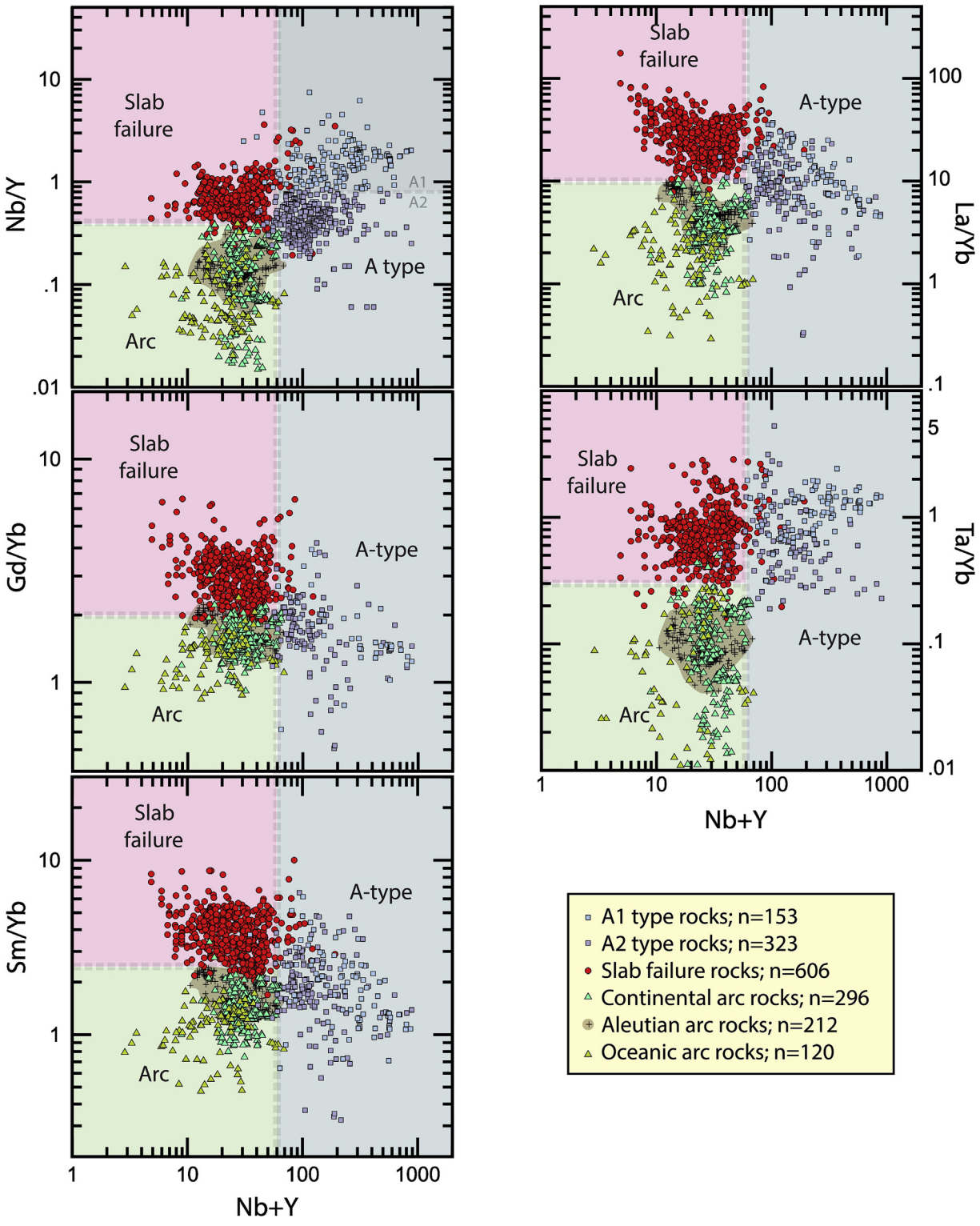

Fig. 7. Y + Nb vs. trace element ratio discrimination plots are used to separate arc, slab failure and A1 and A2 compositions. Shown are the data compilations employed to construct these plots. Separate plots for each granite type compilation are included in Supplementary files C and D, for, due to sample symbol density, it is difficult to evaluate in this figure the amount of overlap between the three granite types, as well as how well the data fit within the granite type fields. Coordinates for plot fields are based on these values: Nb/Y (0.4), Gd/Yb (2.0), Sm/Yb (2.5), Gd/Yb (2.0), La/ Yb (10), Ta/Yb (0.3) and Nb + Y (60).

an example, of 259 >70 wt. % SiO_2 that exhibit slab failure signatures,12% plot in the arc fields and for 60 high silica arc samples, 5% plot as slab failure rocks, a significantly poorer fit than for the <70 wt. % SiO_2 sample subset. In general, we conclude that these new discrimination plots provide a remarkably good fit to the geochemical compilations on which they are based. This is not a circular argument, as initially plutonic suites were identified as being of arc-, slab failure- or A-type on the basis of geological information (see Hildebrand and Whalen, 2017), then on their geochemistry.

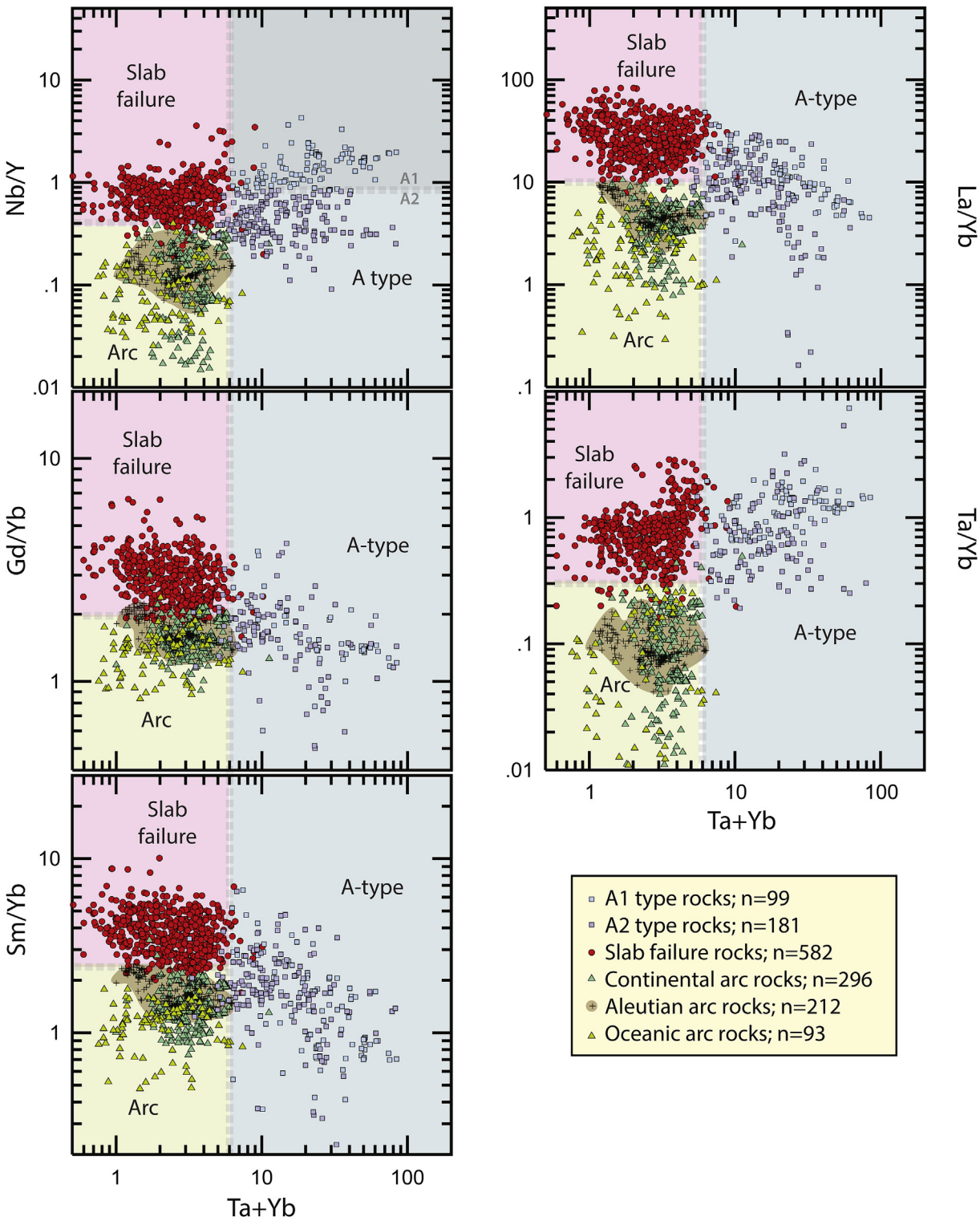

Fig. 8. Yb + Ta vs. trace element ratio discrimination plots are used to separate arc, slab failure and A1 and A2 compositions. See Fig. 7 caption for further information. Coordinates for diagram fields are based on the same values as Fig. 7 except for Yb + Ta (6).

10. Other tectonomagmatic granitoid classification schemes – A discussion

The multicomponent (Fe* (FeOtotal/(FeOtotal + MgO)), MALI (Na_2O+K_2O-CaO) and ASI (mol. Al/(Ca+Na+K-1.67*P)<1.0) scheme (Frost et al., 2001; Frost and Frost, 2008) enables comparison and discussion of granitic rocks without resorting to genetic or tectonic preconceptions. As well, they suggested the scheme be employed to infer tectonic settings (Table 1 in Frost et al., 2001). For magnesian suites, these are outboard- (herein primitive oceanic arc), main- (herein continental arc), and inboard- (herein slab failure +/- S-types) portions of Cordilleran batholiths. Ferroan suites are non-orogenic/ intraplate granite types (our A-type). To evaluate our new classification scheme in the context of this earlier approach,

Table 1
Histogram derived statistics for slab failure trace element ratios.

Granitoid group or compilation	Silica range	La/Yb	SD	N	Sr/Y	SD	N	Nb/Y	SD	N	Ta/Yb	SD	N	Gd/Yb	SD	N	Sm/Yb	SD	N	Y+Nb	SD	N	Yb+Ta	SD	N
Metaluminous SF compilation	55 to 70	22.7	7.9	269	34.0	9.3	169	0.72	0.23	294	0.67	0.23	283	2.97	0.66	297	3.95	1.09	333	20.0	8.0	335	1.84	0.85	333
Metaluminous SF compilation	>70	27.9	9.2	48	26.1	12.5	47	0.94	0.33	76	0.91	0.26	72	2.45	0.93	86	3.48	1.42	97	15.0	11.0	101	1.45	1.61	98
Metaluminous to peraluminous SF compilation	55 to 70	29.4	11.8	245	22.9	10.5	222	0.73	0.29	203	0.78	0.30	197	2.91	0.87	233	3.70	1.18	248	41.0	21.0	304	3.63	1.37	257
Metaluminous to peraluminous SF compilation	>70	23.3	14.7	276	10.9	9.8	264	0.76	0.35	196	0.76	0.32	182	2.49	1.07	232	2.93	1.48	274	47.0	2.8	299	4.96	3.12	287
S-type leucogranite and gneiss compilation	65 to 80	11.5	9.2	280	6.4	6.5	309	0.59	0.32	221	0.69	0.40	145	2.40	1.44	303	3.46	2.37	306	35.8	17.2	311	3.87	3.10	310
Arc compilation	55 to 70	4.2	1.8	296	10.9	4.6	291	0.16	0.10	258	0.13	0.08	268	1.63	0.29	288	1.49	0.39	296	36.0	12.0	292	3.60	1.10	296
Arc compilation	>70	4.5	2.1	76	6.6	5.6	81	0.18	0.08	74	0.02	0.02	67	1.32	0.22	76	1.31	0.29	76	34.0	9.0	61	4.42	1.38	61
Aleutian arc compilation	55 to 70	5.2	1.8	212	17.3	9.2	202	0.14	0.05	212	0.09	0.03	200	1.66	0.24	212	1.67	0.31	212	28.0	11.0	212	2.79	1.13	212
Oceanic and ophiolitic arc compilation	55 to 70	2.7	1.2	60	15.3	8.8	76	0.09	0.06	76	0.12	0.08	43	1.41	0.27	60	1.24	0.24	60	20.0	10.0	77	2.00	1.15	60
Combined A1&A2 compilations	all	10.8	6.9	246	0.96	1.96	464	0.56	0.32	398	0.82	0.38	182	1.71	0.62	162	1.98	0.97	248	111.0	36.0	346	10.80	4.09	188
Arc versus Slab Failure dividing value	55 to 70	10.0			10.0			0.40			0.30			2.00			2.50								

*In this table, for each trace element ratio, the average/mean, standard deviation (SD) and number of samples (N) are given. These values were derived from the histograms shown in Appendix 3.
For example, for the metaluminous slab failure compilation of 55–70 silica samples, the average La/Yb value is 22.7+/-7.9, based on 269 samples.Of note is the statistics are based on the range of the histogram X-axis NOT the full dataset.

we plotted our three main granite types on these multicomponent plots (Fig. 9). We already employed silica and their multicomponent parameter ASI to filter our datasets so as to exclude S-type granites and slab failure plus arc samples with >70 wt. % SiO_2 (Figs. 3 and 5) from the new discrimination plots (Figs. 7 and 8). On the MALI plot the slab failure data set displays a large range from calcic through to alkaline compositions with considerable scatter. In contrast, the vast majority of the arc data are more tightly clustered, falling mainly in the calcic to calc-alkalic fields. On the Fe* plot, of 556 slab failure samples, 96% (535) plot in the magnesian field showing their oxidized nature. In contrast, the 813 arc samples straddle this Fe* boundary. Both arc and slab failure samples with >70 wt. % SiO_2 (N = 320) also broadly straddle this boundary, suggesting that designating a suite as magnesian or ferroan should be based on how samples with <70 wt. % SiO_2 plot on this diagram. On the MALI plot, the A-type granite data spans the calc-alkalic to alkalic fields, whereas on the Fe* plot, 468 of 477 (98%) samples plot in the ferroan field, supporting the suggestion of Frost and Frost (2011) that the term A-type be replaced by 'ferroan granites'. However, although all A-types granites may be ferroan, it was not established by Frost and Frost (2011) that all ferroan granites are enriched in high field strength elements such as Nb, Ta, Y, Zr and HREE, which is the main defining characteristic of A-type granites (Whalen et al., 1987). In summary, as demonstrated by their wide acceptance and usage, the major element multicomponent (MALI, Fe* and ASI) scheme is a valuable tool for characterizing, comparing and contrasting the major element features of granitic suites, but they do not indicate tectonic setting. Combining this major element approach with our trace element based approach when studying granitoid suites of unknown affinity should provide more robust answers concerning basic questions about petrogenesis and tectonic setting than if only one approach was employed in isolation.

The still widely employed trace element classification scheme of Pearce et al. (1984) subdivides granitoid rocks into orogenic (volcanic arc; syn-collisional; and post-collisional) and non-orogenic (within-plate and oceanic-ridge) granitoid rock types. This scheme was re-evaluated by Pearce (1996) as regards the relationships between sources/protoliths and tectonic setting as the original scheme was strongly criticized for reflecting magmatic sources rather than tectonic setting (cf. Förster et al., 1997). We plotted our silica and ASI filtered datasets for arc, slab failure and A-type rocks on the original Pearce et al. (1984) plots (not shown) and found that their field boundaries did not adequately separate these three main granite types. Therefore, we redefined the field boundaries based firstly on our Nb/Y (0.4), Ta/Yb (0.3), Nb + Y (60) and Ta + Yb (6) values and secondly by visually manipulating the boundaries to maximize correspondence to the available data (Fig. 10). Co-ordinates for the fields in these modified plots are given in the caption for Fig. 10 and readily downloaded and utilized versions of these discrimination plots are included in Supplementary file D. Justification for not plotting strongly peraluminous S-type compositions on our modified Pearce discrimination plots is provided by the observation that the compiled S-type samples scatter on plots from well above (higher Rb, Nb and Ta) to completely overlapping the slab failure fields at similar X-values (Fig. 11).

Previously published versions of the Y vs Nb and Yb vs Ta Pearce et al. (1984) plots with modified field boundaries to fit pre- and post-collisional data from the Peninsular Ranges Batholith are presented in Fig. 2c and Supplementary file A. Major differences between these modified plots and the originals are that: (1) the revised plots include slab failure rocks and exclude S-type granites, two-mica leucogranites and ocean ridge granites; (2) except for A-types, samples with >70 wt. % SiO_2 are excluded; and (3) the revised plots are based on ~2580 (mostly ICP-MS) analyses, as

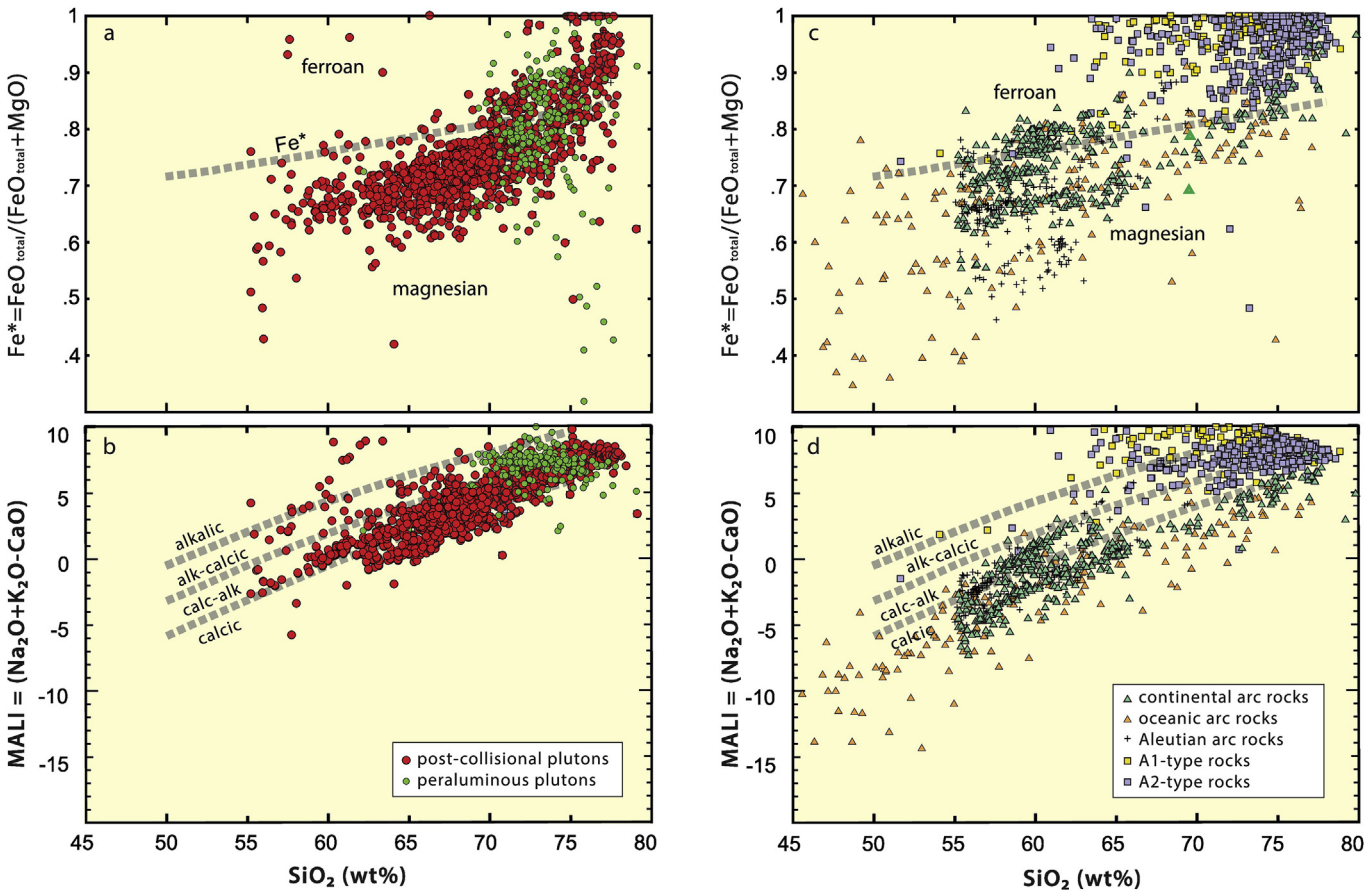

Fig. 9. Multicomponent (a, c) Fe* (FeOtotal/ (FeOtotal + MgO) and (b, d) MALI (Na_2O+K_2O- CaO) vs. silica plots of Frost et al. (2001) and Frost and Frost (2008) for our slab failure (a, b) and arc plus A-type (c, d) compilations.

opposed to the ~600 (mostly XRF) analyses available for the original versions. The only trace element employed by Pearce et al. (1984) that we did not also employ in the revised plots (Figs. 7, 8) is Rb, an element known to be mobile in late-stage fluids or during post-solidification alteration. In our modified Rb vs. Y + Nb and Ta + Yb plots (Fig. 10), the zone of overlap between arc and slab failure compositions may reflect such Rb mobility, so the plots employing Rb should be utilized with caution.

11. Slab failure granitoid rocks: Archean to recent examples

1. Archean sodic leuco-granitoids, usually termed the TTG (tonalite–trondhjemite– granodiorite) series or suite, are estimated to represent at least two-thirds of surviving Archean continental crust (Condie, 1981; Martin, 1994). Hildebrand et al. (2018) recognized that Archean TTG's have similar trace element signatures to younger slab failure rocks (Fig. 12a) and suggested that TTG's are not related to contemporaneous subduction accompanied by slab melting or other competing arc-based models, but instead are products of post-collisional slab failure.
2. Large volume Paleoproterozoic plutonic belts, such as the 70,000 km^2 Wathaman and 221,000 km^2 Cumberland batholiths of the Trans-Hudson Orogen, were interpreted as Andean-type batholiths generated by subduction (e.g. Hoffman, 1988; Meyer et al., 1992; St-Onge et al., 2006). Although modern ICPMS trace element data is sparse, those of MacHattie (2001) collected in a transect across the central portion of the Wathaman Batholith, exhibit exclusively slab failure, not arc, signatures (Fig. 12b) as do many samples collected along a transect across the Cumberland Batholith of Baffin Island (Whalen et al., 2010), suggesting it too was largely generated by slab failure.
3. The Newfoundland Appalachians and Scottish Caledonides preserve cross sections across the former Iapetan tract, where the history includes several accretionary events, each followed by slab failure magmatism. Among the best studied is the accretion of the Middle Ordovician Notre Dame arc to Laurentia as exposed in west-central Newfoundland (van Staal et al., 2007). There, the collision was followed by abundant high Sr/Y and La/Yb tonalitic to granodioritic magmatism interpreted as slab failure magmatism (Whalen, 2012; Whalen et al., 1997). Twenty-two million years of Siluro-Devonian magmatism in the Grampian terrane of Scotland and Ireland postdates the 430 Ma collision of Avalonia with Laurentia and was attributed to slab break-off during the terminal phase of collision (Neilson et al., 2009). In keeping with their post-collisional emplacement, both the Notre Dame and Grampian suites exhibit slab failure geochemical features (Fig. 12c).
4. Post-collisional 'adakitic' granitoid rocks in Tibet and southern China were the subject of numerous geochemical and isotopic studies that produced large publically available datasets (Hou et al., 2015; Lu et al., 2015, 2017). The non-mineralized adakitic samples from Tibet and China plot in tight clusters, almost

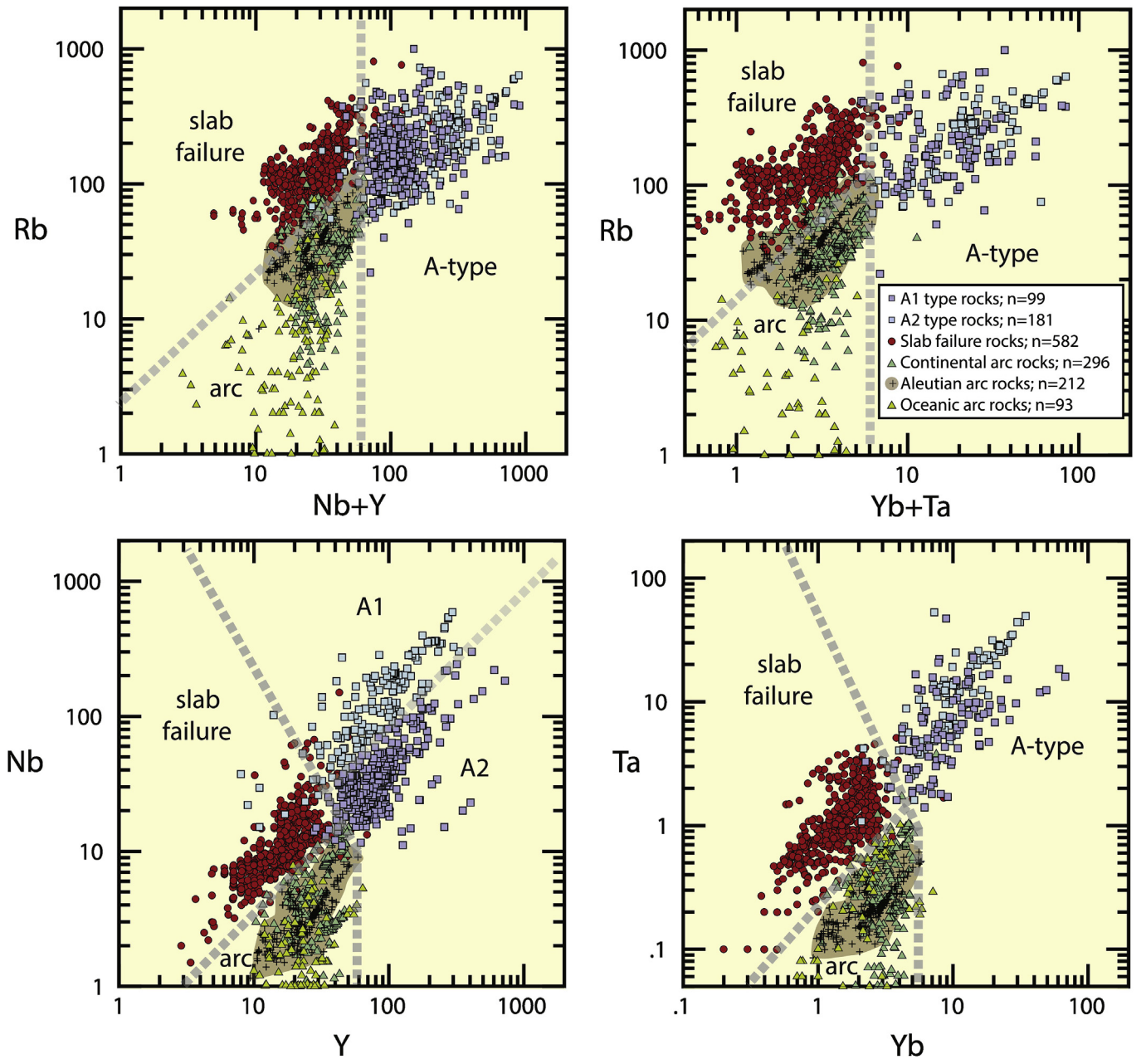

Fig. 10. Pearce et al. (1984) granitoid rock discrimination plots modified to better discriminate between I-type arc, slab failure and A1- and A2-type granitoid compositions. Shown plotted are our datasets filtered remove samples with ASI > 1.1 (i.e. S-types). Due to the relative mobility of Rb in late fluids, behavior not exhibited by the comparatively immobile trace elements Nb, Ta, Y and Yb, caution should be used in utilizing the Rb plots. It is notable that the modified Nb vs. Y and Ta vs. Yb plots offer the advantage of tectonomagmatic classification based on only two trace elements, whereas four out of six of the new discrimination plots require four trace elements. Co-ordinates of the discriminant boundaries are: for the Rb-Y+Nb diagram: SF/Arc = (1,2.5) to (60,120); A-type/SF+Arc = (60,1) to (60,2000); for the Rb-Yb+Ta diagram: SF/Arc = (1,6) to (6,120); A-type/SF+Arc = (6,1) to (6,2000); for the Nb-Y diagram: Arc/SF (3,1) to (40,16); Arc/A2 = (60,1) to (60,10); SF/A1+A2 = (3,2000) to (40,16) ; A1/A2 = (30,30) to (2000,2000); for the Ta-Yb diagram: SF/Arc = (0.3,0.05) to (4.8,1.5); Arc/A-type = (5.5, 0.05) to (5.5, 1); SF/A-type = (0.6, 200) to 5.5, 1). Abbreviations: SF = slab failure.

all falling within the lower right corner of the slab failure fields (Fig. 12d).

12. Slab failure magmas: progenitors to mineralization?

The classification and petrogenesis of high La/Yb and Sr/Y magmas in arc settings and their possible role as progenitors to porphyry Cu-Au-Mo mineralization has been a long standing subject of debate in economic geology (e.g. Baldwin and Pearce, 1982; Richards et al., 2012; Richards and Kerrich, 2007). Richards plus coworkers argued that few high Sr/Y mineralized porphyry intrusions can be convincingly demonstrated to be derived by slab melting. Instead they suggested that such magmas represent natural products of arc maturation accompanied by thickening and melting within the sub-arc lithosphere, with high Sr/Y signatures generated by a combination of high water content, high pressure, and high oxidation state. Alternative models for these magmas include collisional thickening and/or ridge subduction (Hollings et al., 2005), as well as changes in slab dip and subduction erosion (Kay et al., 2005). Basically earlier workers inferred that mineralized high Sr/Y and La/Yb plutonic systems were pre-collisional products of active subduction in an arc setting (see Wilkinson (2013) for a review of this model). In contrast to this arc

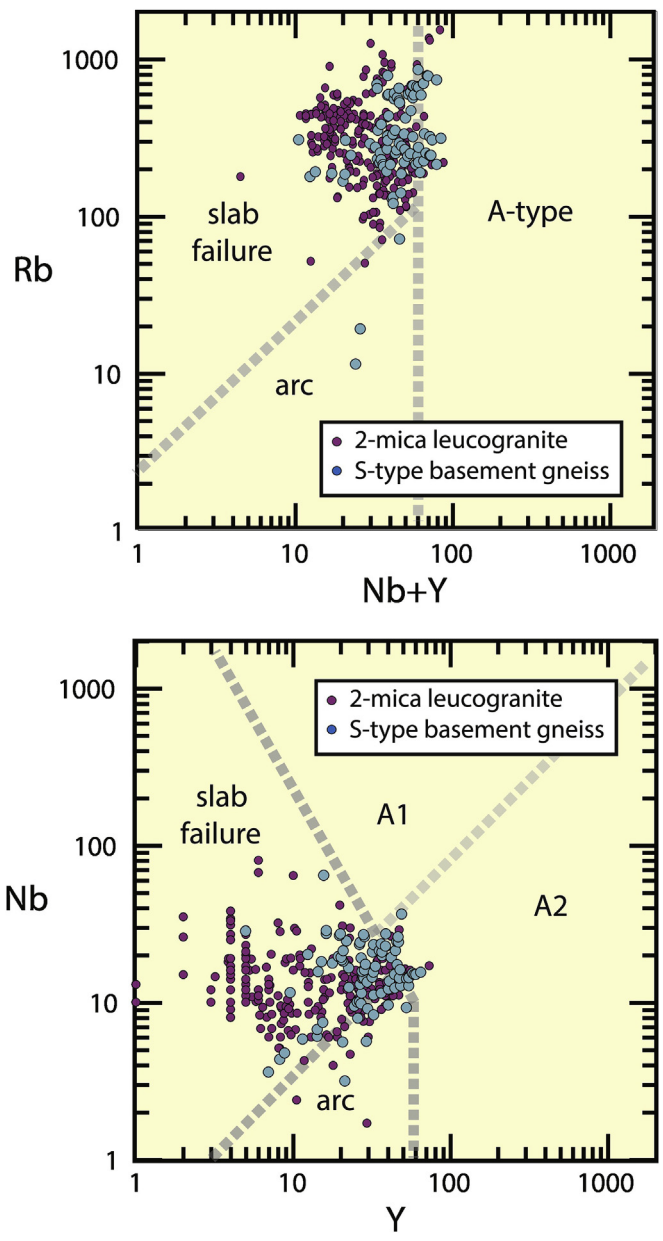

Fig. 11. Post-collisional two-mica leucogranites and Himilayan S-type basement gneisses plotted on the modified (Pearce et al., 1984) Rb vs. Y + Nb and Nb vs. Y plots. We attribute the vertical scatter across multiple fields exhibited by this dataset as due to residual garnet in granulitic residues left from partial melting of sedimentary sources. These plots illustrate how S-type granites can exhibit similar trace element features to slab failure granites when plotted on these diagrams, thus only I-type granite samples with 55–70 wt. % SiO_2 and ASI < 1.1 should be plotted.

model, Chinese researchers in Tibet and southern China recognized early on that the abundant, frequently mineralized, 'adakitic' intrusions in these collisional belts were emplaced post-accretion, and thus not tied to contemporaneous subduction (e.g. Hou et al., 2015; Ma et al., 2015; Wang et al., 2014a, 2014b; Yang et al., 2015, 2016; Zhang et al., 2014). In the literature it is notable that Sr/Y is considered to be just as important an 'adakite discriminator' as La/Yb. However, Hildebrand and Whalen (2017) found that in rocks with SiO_2 >55 wt. %, Sr/Y is subject to alteration by aqueous fluids, and that above 70 wt. % SiO_2 even La/Yb commonly reflects fluid alteration. By using more robust discriminators and their post-deformational nature Hildebrand and Whalen (2017) interpreted these mineralized 'adakitic-like' systems to be post-collisional products of slab failure.

1. The Eocene-Oligocene Kerman batholith of central Iran (Shafiei et al., 2009) illustrates the progression from barren arc-related diorite and granodiorite to post-collisional plutons with associated porphyry deposits (Fig. 13).
2. The Arizona Laramide porphyry Cu-Au district (Lang and Titley, 1998) is one of the richest porphyry districts in the world. Plutons of the district have slab failure signatures (Fig. 13) and are post-tectonic with respect to the Laramide deformation (Hildebrand, 2009).
3. Both the Cu-Au-bearing igneous intrusions of the Gunun Bijih (Ertsberg) District,

Irian Jaya (Cloos et al., 2005; Housh and McMahon, 2000; McMahon, 2000, 2001) and Oki Tedi deposit, Papua New Guinea (Doucette, 2000) are post-collisional. Samples from their host intrusive suites plot in tight clusters within the slab failure fields (Fig. 13).

4. Mineralized post-collisional adakitic samples from Tibet (Lu et al., 2015, 2017) and China (Hou et al., 2015) plot in tight clusters, mostly within the lower right corner of the slab failure fields (Figs. 12, 13).

13. Summary

1. We compiled modern trace element analyses from active arcs, slab failure settings and A-type granitoids. These data were used to refine older elemental ratio discrimination plots to show that arc and slab failure rocks can be reliably separated using Nb/Y, Ta/Yb, La/Yb, Gd/Yb and Sm/Yb. Both arc and slab failure rocks are readily separated from A-type granites using Nb + Y and Ta + Yb. By applying trace element ratio values, researchers can now quickly filter granitoid datasets of unknown tectonic affinity for arc, slab failure and A-type compositions in spreadsheets prior to plotting on classification plots.
2. S-type granites exhibit elevated 'slab failure-like' values for La/Yb, Gd/Yb, Sm/Yb and Nb/Y, but have low Sr/Y values as might be inferred from a granulitic source containing plagioclase and garnet. Based on this finding, and the possibility that many plutonic samples containing less that 55 wt. % SiO_2 are cumulate rocks that do not represent liquid compositions, we concluded that our trace element ratio plots should be restricted to I-type rocks with 55-70 wt. % SiO_2 and aluminum saturation index <1.1, unless they have Y + Nb > 60 ppm and Ta + Yb > 6 ppm as those rocks are A-types.
3. Samples of arc, slab failure and A-type rocks are not adequately classified on the widely used Nb/Y, Ta/Yb, Rb/(Nb + Y) and Rb/(Ta + Yb) plots of Pearce et al. (1984), so field boundaries in these plots were revised in accordance with our worldwide data compilation. The modified plots readily divide I-type granitoid datasets by tectonic setting but, like other discrimination plots, plotting S-type felsic granitoids is not useful.
4. We looked at plutonic rocks from the Archean to Cenozoic and found that rocks of the Precambrian tonalite-trondjhemite-granite suite, as well as large volume Paleoproterozoic plutonic belts, such as the Wathaman and Cumberland batholiths of the Trans-Hudson Orogen, are all compositionally similar to the Cretaceous slab failure reference suites and are likely products of post-collisional slab break-off, rather than arc magmatism. Likewise post-collisional rocks of the Lower Paleozoic Newfoundland Appalachians and Scottish Caledonides, as well as Cenozoic post-collisional granitoid rocks in Tibet and southern China have typical slab failure trace element ratios.
5. Plutons associated with porphyry Cu-Au deposits, such as the Iranian Kerman Cu-Au porphyry camp, the Arizona Laramide

Table 2
Summary of degree of fit of data compilations to new discrimination plots.

Granitoid group or compilation	Silica range	La/Yb			Nb/Y			Ta/Yb			Gd/Yb			Sm/Yb			Y+Nb			Yb+Ta		
		N	<9.5	%	N	<0.35	%	N	<0.25	%	N	<1.8	%	N	<2.45	%	N	>60.5	%	N	>5.5	%
Metaluminous SF compilation	55 to 70	333	2	0.6	294	4	1.4	286	6	2.1	298	0	0.0	333	13	3.9	336	0	0.0	334	0	0.0
Metaluminous to peraluminous SF compilation	55 to 70	248	0	0.0	217	11	5.1	231	2	0.9	234	1	0.4	250	27	10.8	248	22	8.9	248	16	6.5
S-type leucogranite and gneiss compilation	65 to 80	311	155	49.8	308	59	19.2	224	26	11.6	311	126	40.5	311	147	47.3	311	29	9.3	311	77	24.8
Arc versus Slab Failure dividing value			>10			>0.40			>0.30			>2.0			>2.50			>60.0			>6.0	
Continental arc compilation	55 to 70	296	2	0.7	260	0	0.0	267	4	1.5	288	45	15.6	296	2	0.7	292	8	2.7	296	13	4.4
Aleutian arc compilation	55 to 70	424	0	0.0	424	0	0.0	401	2	0.5	424	54	12.7	424	0	0.0	424	2	0.5	424	19	4.5
Combined arc compilation	>70	61	0	0.0	54	0	0.0	60	3	5.0	61	0	0.0	61	0	0.0	61	0	0.0	61	10	16.4
Oceanic and ophiolitic arc compilation	50 to 70	93	0	0.0	116	0	0.0	66	0	0.0	65	2	3.1	94	0	0.0	94	2	2.1	67	6	9.0
																		<60.0			>6.0	
combined A1&A2 compilations	all																477	19	4.0	246	3	1.2
Arc versus Slab Failure dividing value	55 to 70	10.0			0.4			0.3			2.0			2.5								
SF plus Arc versus A-type dividing value																	60			6		

*Below the discriminating trace element ratios in this table, the number of samples for which there is data is given, followed by the cut off value for non-fit samples, the number of non-fit samples, and the percentage of non-fit samples. As an example, for the metaluminous SF 55−70 silica sample compilation, there are 333 samples with Sm/Yb values of which 13 or 3.9% exhibit values <2.45.
As the available trace elements for each sample varies, the number of samples available for each ratio varies
Abbreviations: SF = slab failure; N = number of samples.

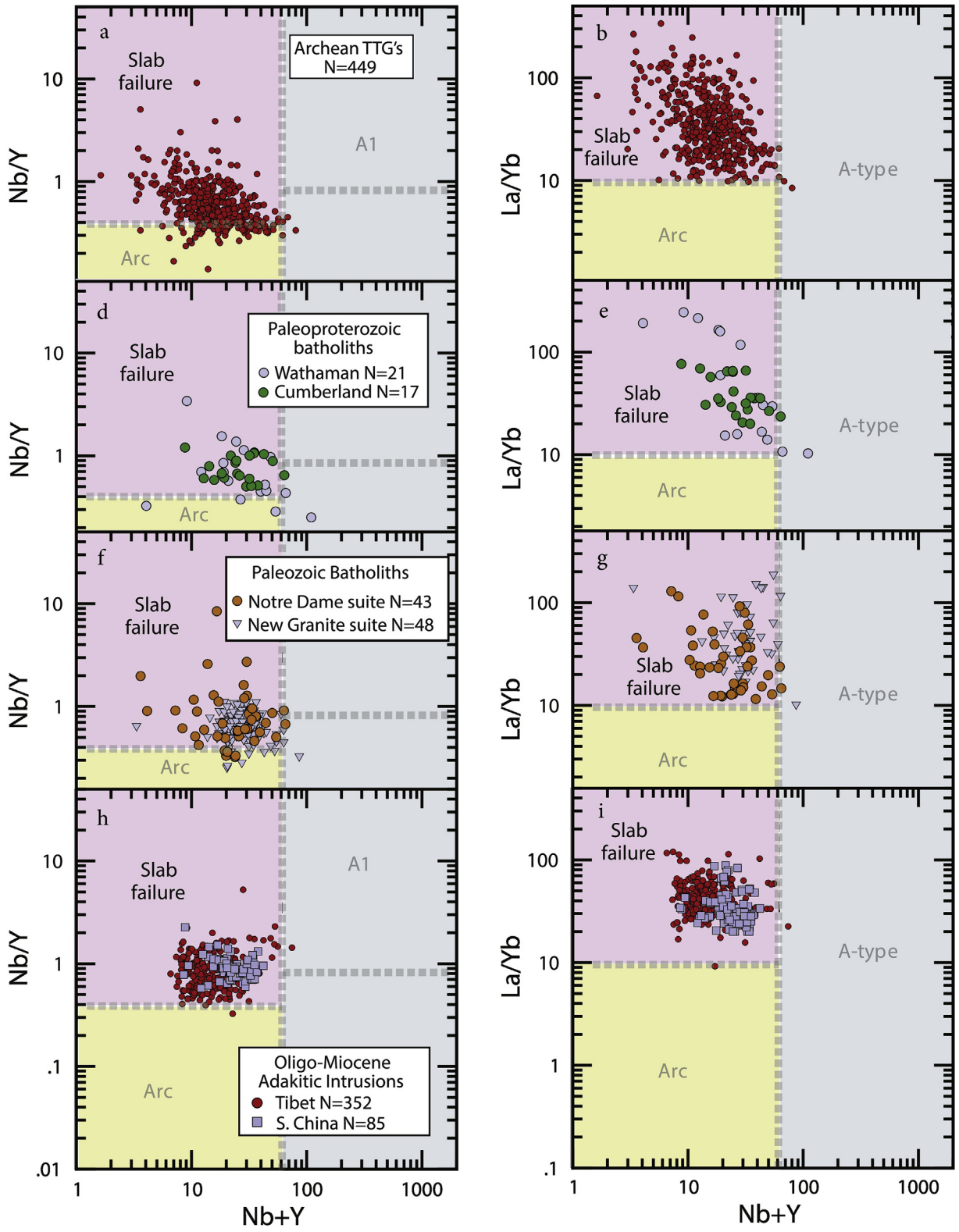

Fig. 12. Y + Nb versus Nb/Y and La/Yb discrimination plots for silica filtered (55-70 wt. %) Archean to Miocene slab failure granitoid suites: (a) Archean sodic granitoids, usually termed the TTG (tonalite–trondhjemite–granodiorite) series or suite (for data sources see Hildebrand et al., 2018); (b) Paleoproterozoic Cumberland and Wathaman batholiths, Trans-Hudson Orogen (Wathaman data from MacHattie (2001), Cumberland data from Whalen et al. (2010)); (c) Ordovician Appalachian and Caledonian slab failure granitoid suites (Notre Dame suite data from Whalen (2012) and Grampian suite (pers. com. 2015 Peter Kokelaar); and; (d) Oligo-Miocene 'adakitic' granitoid suites in Tibet (data compilation of Lu et al. (2017)) and southern China (data compilation of Hou et al. (2015)). These plots help substantiate the widespread distribution and volumetric importance of slab failure plutonism through Earth history. The ratios Sr/Y, Nb/Y and La/ Yb were chosen for these plots because they reflect residual plagioclase (Sr), garnet (Y and Yb) and rutile (Nb).

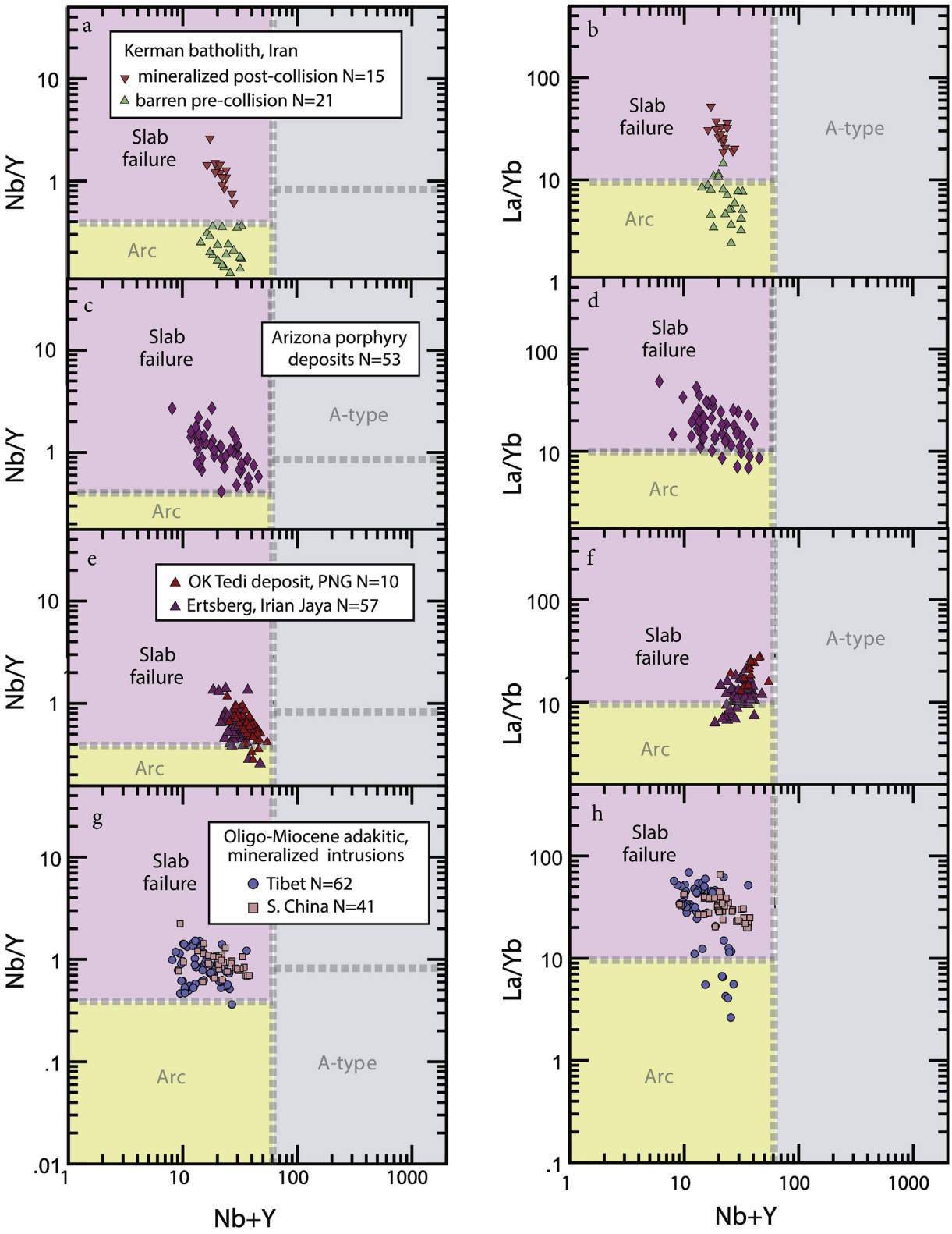

Fig. 13. Y + Nb versus Nb/Y and La/Yb discrimination plots for mineralized slab failure suites: (a) the Kerman batholith, Iran, consists of a pre-collisional barren arc suite and a post-collision mineralized slab failure suite (data from Shafiei et al. (2009)); (b) Larimide Arizona porphyry Cu-Mo and Cu-Au deposit hosting intrusions (data from Lang and Titley, 1998); (c) Oki Tedi deposit intrusions, Papua New Guinea (data of Doucette (2000)) and Ertsberg deposit related intrusive suite, Irian Jaya (data of McMahon (2000, 2001)), Housh and McMahon, 2000); (d) Oligo-Miocene mineralized (mainly Cu-Au) adakitic intrusions in Tibet (data compilation of Lu et al. (2015, 2017)) and southern China (data compilation of Hou et al. (2015)). These plots help substantiate that slab failure magmatism is frequently related to porphyry-type mineralization.

porphyry district, SW Pacific porphyry deposits (Ok Tedi and Ersberg) and common Cu-Au bearing post-collisional intrusive suites in Tibet and China have slab failure trace element signatures. This suggests that epizonal slab failure, not arc, plutons are the better prospect for Cu-Au mineralization.

Acknowledgements

We thank Drs. Nelson Eby and Krishna Sinha for providing us with digital A-type granite geochemical compilations. Also, we thank Dr. Neil Rogers, GSC, for a very constructive review of an earlier version of this manuscript. Drs. D. Davis and R. Dall'Agnol provided very helpful journal reviews that greatly improved the manuscript. This research is self-funded, so it did not receive any grants from funding agencies in the public, commercial, or not-for-profit sectors.

Appendix A. Supplementary data

Supplementary data to this article can be found online at https://doi.org/10.1016/j.lithos.2019.105179.

References

Åberg, G., Aguirre, L., Levi, B., Nyström, J.O., Aguirre, L., 1984. Spreading-subsidence and generation of ensialic marginal basins: an example from the early Cretaceous of central Chile. In: Kokelaar, B.P., Howells, M.F. (Eds.), Marginal Basin Geology: Volcanic and Associated Sedimentary and Tectonic Processes in Modern and Ancient Marginal Basins, pp. 185–193. Geological Society, London, Special Publication 16.

Allison, F.C., 1974. The type Alisitos formation (Cretaceous, Aptian–Albian) of Baja California and its bivalve fauna. In: Gastil, G., Lillegraven, J. (Eds.), Geology of Peninsular California. AAPG-SEPM-SEG Pacific Section 49th Annual Meeting Field Trip Guidebook, pp. 20–59.

Atherton, M.P., Warden, V., Sanderson, L.M., 1985. The Mesozoic marginal basin of central Peru: a geochemical study of within-plate-edge volcanism. In: Pitcher, W.S., Atherton, M.P., Cobbing, E.J., Beckinsale, R.B. (Eds.), Magmatism at a Plate Edge, the Peruvian Andes. Blackie Halstead Press, Glasgow, pp. 47–58.

Baldwin, J.A., Pearce, J.A., 1982. Discrimination of productive and nonproductive porphyritic intrusions in the Chilean Andes. Econ. Geol. 77, 664–674.

Batchelor, R.A., Bowden, P., 1985. Petrogenetic interpretation of granitoid rock series using multicationic parameters. Chem. Geol. 48, 43–55.

Bateman, P.C., 1992. Plutonism in the Central Part of the Sierra Nevada Batholith. U.S. Geological Survey Professional Paper 1483, 186 p.

Bonin, B., 2007. A-type granites and related rocks; evolution of a concept, problems and prospects. Lithos 97, 1–29.

Burk, C.A., 1965. Geology of the Alaskan Peninsula–Island Arc and Continental Margin (Part 1). Geol. Soc. Am. Memoir 99, 265.

Busby-Spera, C.J., 1988. Speculative tectonic model for the early Mesozoic arc of the southwest Cordilleran United States. Geology 16, 1121–1125.

Castro, A., 2014. The off-crust origin of granite batholiths. Geosci. Front. 5, 63–75.

Chappell, B.W., White, A.J.R., 1974. Two contrasting granite types. Pac. Geol. 8, 173–174.

Chappell, B.W., White, J.R., 2001. Two contrasting granite types: 25 years later. Aust. J. Earth Sci. 48, 489–499.

Cloos, M., Sapiie, B., van Ufford, A.Q., Weiland, R.J., Warren, P.Q., McMahon, T.P., 2005. Collisional delamination in New Guinea: the geotectonics of subducting slab breakoff. Geol. Soc. Am. Spec. Pap. 400, 51.

Collins, W.J., Beams, D., White, J.R., Chappell, B.W., 1982. Nature and origin of A-type granites with particular reference to south-eastern Australia. Contrib. Mineral. Petrol. 80, 189–200.

Condie, K.C., 1981. Archaean Greenstone Belts. Elsevier, Amsterdam, p. 434.

Creaser, R.A., Price, R.C., Wormald, R.J., 1991. A-type granites revisited: assessment of a residual-source model. Geology 19, 163–166.

Dall'Agnol, R., Frost, C.D., Tapani Rämö, O., 2012. IGCP Project 510 "A-type Granites and Related Rocks through Time": project vita, results, and contribution to granite research. Lithos 151, 1–16.

Davies, J.H., von Blanckenburg, F., 1995. Slab breakoff: a model of lithosphere detachment and its test in the magmatism and deformation of collisional orogens. Earth Planet. Sci. Lett. 129, 85–102.

Debon, F., LeFort, P., 1983. A chemical-mineralogical classification of common plutonic rocks and associations. Transactions of the Royal Society of Edinburgh. Earth Sci. 73, 135–149.

Doucette, J., 2000. A Petrochemical Study of the Mount Fubilan Intrusion and Associated Ore Bodies, Papua New Guinea. Unpublished Ph.D. thesis. Oregan State University, p. 400.

Druitt, T.H., Francaviglia, V., 1992. Caldera formation on Santorini and the physiography of the islands in the late Bronze Age. Bull. Volcanol. 54, 484–493. https://doi.org/10.1007/BF00301394.

Ducea, M., 2001. The California arc: thick granitic batholiths, eclogitic residues, lithospheric-scale thrusting, and magmatic flare-ups. GSA Today 11, 4–10.

Ducea, M.N., Paterson, S.R., DeCelles, P.G., 2015. High-volume magmatic events in subduction systems. Elements 11, 99–104.

Eby, G.N., 1990. The A-type granitoids: a review of their occurrence and chemical characteristics and speculations on their petrogenesis. Lithos 26, 115–134.

Eby, G.N., 1992. Chemical subdivision of A-type granitoids: petrogenetic and tectonic implications. Geology 20, 641–644.

England, P.C., Thompson, A.B., 1984. Pressure-temperature-time paths of regional metamorphism; I, Heat transfer during the evolution of regions of thickened continental crust. J. Petrol. 25, 894–928.

Förster, H.J., Tischendorf, G., Trumbull, R.B., 1997. An evaluation of the Rb vs. (Y + Nb) discrimination diagram to infer tectonic setting of silicic igneous rocks. Lithos 40, 261–293.

Freeburn, R., Bouilhol, P., Maunder, B., Magni, V., van Hunen, J., 2017. Numerical models of the magmatic processes induced by slab break-off. Earth Planet. Sci. Lett. 478, 203–213.

Frost, B.R., Frost, C.D., 2008. A geochemical classification for feldspathic igneous rocks. J. Petrol. 49, 1955–1969.

Frost, C.D., Frost, B.R., 2011. On ferroan (A-type) granitoids: their compositional variability and modes of origin. J. Petrol. 51, 39–57.

Frost, B.R., Arculus, R.J., Barnes, C.G., Collins, W.J., Ellis, D.J., Frost, C.D., 2001. A geochemical classification of granitic rocks. J. Petrol. 42, 2033–2048.

Gastil, R.G., Kimbrough, D.L., Kimbrough, J.M., Grove, M., Shimizu, M., 2014. The Sierra San Pedro Mártir zoned pluton, Baja California, Mexico. In: Morton, D.M., Miller, F.K. (Eds.), Peninsular Ranges Batholith, Baja California and Southern California. Geological Society of America Memoir 211, pp. 739–758.

Guo, Z., Wilson, M., 2012. The Himalayan leucogranites: constraints on the nature of their crustal source region and geodynamic setting. Gondwana Res. 22, 360–376. https://doi.org/10.1016/j.gr.2011.07.027.

Hamilton, W.B., 1969. The volcanic central Andes, a modern model for the Cretaceous batholiths and tectonics of western North America. Bull. Oregon Dept. Geol. Mineral Ind. 65, 175–184.

Harrison, A., White, R.S., 2006. Lithospheric structure of an active backarc basin: the Taupo volcanic zone, New Zealand. Geophys. J. Int. 167, 968–990. https://doi.org/10.1111/j.1365-246X.2006.03166.x.

Hildebrand, R.S., 2009. Did Westward Subduction Cause Cretaceous–Tertiary Orogeny in the North American Cordillera? Geological Society of America Special Paper 457, 71 p https://doi.org/10.1130/2009.2457.

Hildebrand, R.S., 2015. Dismemberment and northward migration of the Cordilleran orogen: Baja-BC resolved. GSA Today 25 (11), 4–11.

Hildebrand, R.S., Bowring, S.A., 1984. A non-extensional model for the origin of continental intra-arc depressions, with a Proterozoic example from Wopmay orogen, Northwest Territories, Canada. Geology 12, 73–77.

Hildebrand, R.S., Bowring, S.A., 1999. Crustal recycling by slab failure. Geology 27, 11–14.

Hildebrand, R.S., Whalen, J.B., 2014. Arc and Slab-Failure Magmatism in Cordilleran Batholiths I – The Cretaceous Coastal Batholith of Peru and Its Role in South American Orogenesis and Hemispheric Subduction Flip, 41. Paul Hoffman Volume, Geoscience Canada, pp. 255–282.

Hildebrand, R.S., Whalen, J.B., 2014. Arc and slab-failure magmatism in Cordilleran batholiths II – The Cretaceous Peninsular Ranges batholith of Southern and Baja California, 41. Paul Hoffman Volume, Geoscience Canada, pp. 399–458.

Hildebrand, R.S., Whalen, J.B., 2017. The Tectonic Setting and Origin of Cretaceous Batholiths Within the North American Cordillera: The Case for Slab Failure Magmatism and Its Significance for Crustal Growth. Geological Society of America Special Paper 532, 113 p.

Hirt, W.H., 2007. Petrology of the Mount Whitney Intrusive Suite, eastern Sierra Nevada, California: implications for the emplacement and differentiation of composite felsic intrusions. Geol. Soc. Am. Bull. 119, 1185–1200. https://doi.org/10.1130/B26054.1.

Hoffman, P.F., 1988. United plates of America, the birth of a craton: early proterozoic assembly and growth of Laurentia. Annu. Rev. Earth Planet. Sci. 16, 543–603.

Hollings, P., Cooke, D., Clark, A., 2005. Regional geochemistry of Tertiary igneous rocks in central Chile: implications for the geodynamic environment of giant porphyry copper and epithermal gold mineralization. Econ. Geol. 100, 887–904.

Hou, Z., Yang, Z., Lu, Y., Kemp, A., Zheng, Y., Li, Q., Tang, J., Yang, Z., Duan, L., 2015. A genetic linkage between subduction- and collision-related porphyry Cu deposits in continental collision zones. Geology 43, 247–250. Data Repository item 2015088. https://doi.org/10.1130/G36362.1.

Housh, T.B., McMahon, T.P., 2000. Ancient isotopic characteristics of Neogene potassic magmatism in western New Guinea (Irian Jaya, Indonesia). Lithos 50, 217–239.

Johnson, J.A., 2014. A Geochemical Study of Crustal Plutonic Rocks from the Southern Mariana Trench Forearc: Relationship toVolcanic Rocks Erupted during Subduction Initiation. Florida International University (FIU) Electronic Theses and Dissertations 1249. http://digitalcommons.fiu.edu/etd/1249.

Kay, S.M., Godoy, E., Kurtz, A., 2005. Episodic arc migration, crustal thickening, subduction erosion, and magmatism in the south-central Andes. Bull. Geol. Soc. Am. 117, 67–88.

Lackey, J.S., Valley, J.W., Chen, J.H., Stockli, D.F., 2008. Dynamic magma systems, crustal recycling, and alteration in the Central Sierra Nevada Batholith: the oxygen isotope record. J. Petrol. 49, 1397–1426.

Lang, J.R., Titley, S.R., 1998. Isotopic and geochemical characteristics of Laramide magmatic systems in Arizona and implications for the genesis of porphyry copper deposits. Econ. Geol. 93, 138–170.

Lee, C.-T.A., Lackey, J.S., 2015. Global continental arc flare-ups and their relation to

long-term greenhouse conditions. Elements 11, 125–130.
Lee, C.-T.A., Morton, D.M., Kistler, R.W., Baird, A.K., 2007. Petrology and tectonics of Phanerozoic continent formation: from island arcs to accretion and continental arc magmatism. Earth Planet. Sci. Lett. 263, 370–387.
Levin, V., Shapiro, N., Park, J., Ritzwoller, M., 2002. Seismic evidence for catastrophic slab loss beneath Kamchatka. Nature 418, 763–767. https://doi.org/10.1038/nature00973.
Loiselle, M.C., Wones, D.R., 1979. Characteristics and Origin of Anorogenic Granites. Geological Society of America Abstracts with Programs 11, p. 468.
Lu, Y.J., Loucks, R.R., Fiorentini, M.L., Yang, Z.M., Hou, Z.Q., 2015. Fluid flux melting generated post-collisional high Sr/Y copper ore–forming water-rich magmas in Tibet. Geology 43, 583–586. DR2015198 Table DR1.
Lu, Y.J., Hou, Z.Q., Yang, Z.M., Parra-Avila, L.A., Fiorentini, F., McCuaig, T.C., Loucks, R.R., 2017. Terrane-scale porphyry Cu fertility in the Lhasa terrane, southern Tibet. In: TARGET 2017. Abstracts. Geological Survey of Western Australia Record, Perth, Australia, pp. 95–100, 2017/6.
Ma, X., Shu, L., Meert, J.G., 2015. Early Permian slab breakoff in the Chinese Tianshan belt inferred from the post- collisional granitoids. Gondwana Res. 27, 228–243. https://doi.org/10.1016/j.gr.2013.09.018.
MacHattie, T.G., 2001. Petrogenesis of the Wathaman Batholith and La Ronge Domain Plutons in the Reindeer Lake Area, Trans-Hudson Orogen, Saskatchewan. Masters thesis. Memorial University of Newfoundland.
MacLeod, C.J., Lissenberg, C.J., Bibby, L.E., 2013. 'Moist MORB' axial magmatism in the Oman ophiolite: the evidence against a mid ocean ridge origin. Geology 41 (4), 459–462. https://doi.org/10.1130/G33904.1.
Martin, H., 1994. The Archean grey gneisses and the genesis of the continental crust. In: Condie, K.C. (Ed.), The Archean Crustal Evolution. Developments in Precambrian Geology, Elsevier, Amsterdam, pp. 205–259.
McMahon, T.P., 2000. Magmatism in an arc-continent collision zone: an example from Irian Jaya (western New Guinea), Indonesia. Buletin Geologi 32, 1–22.
McMahon, T.P., 2001. Origin of a collision-related ultrapotassic to calc-alkaline magmatic suite: the latest Miocene Minjuah volcanic field, Irian Jaya, Indonesia. Buletin Geologi 33, 47–77.
Memeti, V., 2009. Growth of the Cretaceous Tuolumne Batholith and Synchronous Regional Tectonics, Sierra Nevada, CA: A Coupled System in a Continental Margin Arc Setting. Unpublished PhD thesis. University of Southern California, Los Angeles, CA, p. 282.
Memeti, V., Gehrels, G.E., Paterson, S.R., Thompson, J.M., Mueller, R.M., Pignotta, G.S., 2010. Evaluating the Mojave–Snow Lake fault hypothesis and origins of central Sierran metasedimentary pendant strata using detrital zircon provenance analyses. Lithosphere 2, 341–360.
Meyer, M.T., Bickford, M.E., Lewry, J.F., 1992. The Wathaman batholith: an early Proterozoic continental arc in the Trans-Hudson orogenic belt, Canada. Geol. Soc. Am. Bull. 104, 1073–1085.
Morton, D.M., Miller, F.K., 2014. Peninsular Ranges Batholith. Baja California and Southern California. Geological Society of America Memoir 211, p. 758.
Moyen, J.-F., 2009. High Sr/Y and La/Yb ratios: the meaning of the "adakitic signature". Lithos 112, 556–574.
Neilson, J.C., Kokelaar, B.P., Crowley, Q.G., 2009. Timing, relations and cause of plutonic and volcanic activity of the Siluro-Devonian post-collision magmatic episode in the Grampian Terrane, Scotland. J. Geol. Soc. Lond. 166, 545–561.
Pearce, J.A., 1996. Sources and settings of granitic rocks. Episodes 19, 120–125.
Pearce, J.A., 2014. Immobile element fingerprinting of ophiolites. Elements 10, 101–108, 10.2113/gselements.10.2.101.
Pearce, J.A., Harris, N.B.W., Tindle, A.G., 1984. Trace element discrimination diagrams for the tectonic interpretation of granitic rocks. J. Petrol. 25, 956–983.
Pitcher, W.S., 1993. The Nature and Origin of Granite. Blackie Academic, London, p. 321. https://doi.org/10.1007/978-94-017-3393-9.
Power, J.A., Coombs, M.L., Freymueller, J.T., 2010. The 2006 Eruption of Augustine Volcano, Alaska. USGS Professional Paper 1769, p. 667.
Putirka, K.D., 1999. Melting depths and mantle heterogeneity beneath Hawaii and the East Pacific Rise: constraints from Na/Ti and rare earth element ratios. J. Geophys. Res. 104, 2817–2829.
Richards, J.P., Kerrich, R., 2007. Adakite-like rocks: their diverse origins and questionable role in metallogenesis. Econ. Geol. 102, 537–576.
Richards, J.P., Spell, T., Rameh, E., Raziques, A., Flectcher, T., 2012. High Sr/Y magmas reflect arc maturity, high magmatic water content, and porphyry Cu ± Mo ± Au potential: examples from the Tethyan arcs of central and eastern Iran and western Pakistan. Econ. Geol. 107, 295–332.
Rollinson, H., 2009. New models for the genesis of plagiogranites in the Oman ophiolite. Lithos 112, 603–614. https://doi.org/10.1016/j.lithos.2009.06.006.
Sacks, P.E., Secor Jr., D.T., 1990. Delamination in collisional orogens. Geology 18, 999–1002.
Saleeby, J.B., Ducea, M.N., Busby, C.J., Nadin, E.S., Wetmore, P.H., 2008. Chronology of pluton emplacement and regional deformation in the southern Sierra Nevada batholith, California. In: Wright, J.E., Shervais, J.W. (Eds.), Ophiolites, Arcs, and Batholiths: A Tribute to Cliff Hopson, pp. 397–427. Geological Society of America Special Paper 438.
Shafiei, B., Haschke, M., Shahabpour, J., 2009. Recycling of orogenic arc crust triggers porphyry Cu mineralization in Kerman Cenozoic arc rocks, southeastern Iran. Mineral. Deposita 44, 265–283.
Shervais, J.W., 2001. Birth, death, and resurrection: The life cycle of suprasubduction zone ophiolites. Geochem. Geophys. Geosyst. 2, 2000GC000080.
Shervais, J.W., 2008. Tonalites, trondhjemites, and diorites of the Elder Creek ophiolite, California: low-pressure slab melting and reaction with the mantle wedge. In: Wright, J.E., Shervais, J.W. (Eds.), Ophiolites, Arcs, and Batholiths: A Tribute to Cliff Hopson, pp. 113–132. https://doi.org/10.1130/2008.2438(03). Geological Society of America Special Paper 438.
Simons, B., Shail, R.K., Andersen, J.C.Ø., 2016. The petrogenesis of the Early Permian Variscan granites of the Cornubian Batholith: lower plate post-collisional peraluminous magmatism in the Rhenohercynian Zone of SW England. Lithos 260, 76–94. https://doi.org/10.1016/j.lithos. 2016.05.010.
St-Onge, M.R., Searle, M.P., Wodicka, N., 2006. Trans-Hudson Orogen of North America and Himalaya– Karakoram–Tibetan orogen of Asia: structural and thermal characteristics of the lower and upper plates. Tectonics 25. TC4006, 22 pp.
Stowall, H., Rusmore, M., Woodsworth, G., 2019. Processes controlling the growth and evolution of continental batholiths, Coast Mountains, British Columbia, Canada. GSA Today 20 (3-4), 20–22.
Till, C.B., Grove, T.L., Krawczynski, M.J., 2012. A melting model for variably depleted and enriched lherzolite in the plagioclase and spinel stability fields. J. Geophys. Res. Solid Earth 117, B06206.
Ulmer, P., 2001. Partial melting in the mantle wedge — the role of H2O in the genesis of mantle-derived 'arc- related' magmas. Phys. Earth Planet. Inter. 127, 215–232.
Van Buer, N.J., Miller, E.L., 2010. Sahwave batholith, NW Nevada: cretaceous arc flare-up in a basinal terrane. Lithosphere 2, 423–446. https://doi.org/10.1130/L105.1.
van Staal, C.R., Whalen, J.B., McNicoll, V.J., Pehrsson, S., Lissenberg, C.J., Zagorevski, A., van Breemen, O., Jenner, G., 2007. The Notre Dame Arc and the Taconic Orogeny in Newfoundland. In: Hatcher Jr., R.D., Carlson, M.P., McBride, J.H., Martinez Catalan, J.R. (Eds.), 4-D Framework of Continental Crust, pp. 511–552. Geological Society of America Memoir 200,.
Wang, R., Richards, J.P., Hou, Z., Yang, Z., DuFrane, S.A., 2014. Increased magmatic water content - The key to Oligo-Miocene porphyry Cu-Mo±Au formation in the eastern Gangdese Belt, Tibet. Econ. Geol. 109, 1315–1339.
Wang, R., Richards, J.P., Hou, Z., Yang, Z., Guo, Z., DuFrane, S.A., 2014. Increasing magmatic oxidation state from Paleocene to Miocene in the eastern Gangdese Belt, Tibet: implications for collision-related porphyry Cu-Mo±Au mineralization. Econ. Geol. 109, 1943–1965.
Whalen, J.B., 1985. Geochemistry of an island-arc plutonic suite: the Uasilau-Yau Yau intrusive complex, New Britain, P.N.G. J. Petrol. 26, 603–632. https://doi.org/10.1093/petrology/26.3.603.
Whalen, J.B., 2012. Geochemical and Isotopic (Nd, O, Pb and Sr) Data from Igneous Rocks of the Notre Dame subzone and adjacent tectonostratigraphic zones, western and central Newfoundland. Geological Survey of Canada, Open File 7202, 1 zip file. https://doi.org/10.4095/291593.
Hildebrand, R.S., Whalen, J.B., Bowring, S.A., 2018. Resolving the crustal composition paradox by 3.8 billion years of slab failure magmatism and collisional recycling of continental crust. Tectonophysics 734–-725, 69–88.
Whalen, J.B., Frost, C.D., 2013. The Q-ANOR Diagram: A Tool for the Petrogenetic and Tectonomagmatic Characterization of Granitic Suites. Geological Society of America, Abstracts with Programs 45, no. 3, p. 24.
Whalen, J.B., Currie, K.L., Chappell, B.W., 1987. A-type granites: geochemical characteristics, discrimination and petrogenesis. Contrib. Mineral. Petrol. 95, 407–419.
Whalen, J.B., Jenner, G.A., Longstaffe, F.J., Robert, F., Gariépy, C., 1996. Geochemical and isotopic (O, Nd, Pb and Sr) constraints on A-type granite petrogenesis based on the Topsails igneous suite, Newfoundland Appalachians. J. Petrol. 37, 1463–1489.
Whalen, J.B., Jenner, G.A., Longstaffe, F.J., Gariépy, C., Fryer, B.J., 1997. Implications of granitoid geochemical and isotopic (Nd, O, Pb) data from the Cambro-Ordovician Notre Dame arc for the evolution of the Central Mobile Belt, Newfoundland Appalachian. In: Sinha, A.K., Whalen, J.B., Hogan, J. (Eds.), Magmatism in the Appalachian Orogen, pp. 367–395. Geological Society of America Memoir 191.
Whalen, J.B., McNicoll, V.J., van Staal, C.R., Lissenberg, C.J., Longstaffe, F.J., Jenner, G.A., van Breeman, O., 2006. Spatial, temporal and geochemical characteristics of Silurian collision-zone magmatism, Newfoundland Appalachians: an example of a rapidly evolving magmatic system related to slab break-off. Lithos 89, 377–404.
Whalen, J.B., Wodicka, N., Taylor, B.E., Jackson, G.A., 2010. Cumberland batholith, Trans Hudson Orogen, Canada: petrogenesis and implications for Paleoproterozoic crustal and orogenic processes. Lithos 117, 99–118.
Whalen, J.B., Berman, R.G., Davis, W.J., Sanborn-Barrie, M., Nadeau, L., 2018. Bedrock geochemistry of the Thelon tectonic zone, Nunavut. Geological Survey of Canada, Open File 8234, 1 zip file. https://doi.org/10.4095/306385.
Wilkinson, J.J., 2013. Triggers for the formation of porphyry ore deposits in magmatic arcs. Nat. Geosci. 6, 917–925.
Williams, H., McBirney, A.R., 1979. Volcanology. California, Freeman, Cooper and Co, San Francisco, p. 397.
Wilmsen, M., Fürsich, F.T., Seyed-Emami, K., Majidifard, M.R., Taheri, J., 2009. The Cimmerian Orogeny in northern Iran: tectono-stratigraphic evidence from the foreland. Terra Nova 21, 211–218. https://doi.org/10.1111/j. 1365- 3121.2009.00876.x.
Windley, B.F., 1993. Proterozoic anorogenic magmatism and its orogenic connections. J. Geol. Soc. Lond. 150, 39–50.
Yang, Z.M., Lu, Y.J., Hou, Z.Q., Chang, Z.S., 2015. High-Mg diorite from Qulong in southern Tibet: implications for the genesis of adakite- like intrusions and associated porphyry Cu deposits in collisional orogens. J. Petrol. 56, 227–254.
Yang, Z.M., Goldfarb, R., Chang, Z.S., 2016. Generation of Postcollisional Porphyry Copper Deposits in Southern Tibet Triggered by Subduction of the Indian Continental Plate. Society of Economic Geologists Special Publication 19, pp. 279–300.
Zhang, L.Y., Ducea, M.N., Ding, L., Pullen, A., Kapp, P., Hoffman, D., 2014. Southern Tibetan Oligocene–Miocene adakites: a record of Indian slab tearing. Lithos 210–211, 209–223. https://doi.org/10.1016/j.lithos.2014.09.029.